Geochemistry Geophysics Geosystems G3

Published by AGU and the Geochemical Society

Article
Volume 13, Number 10
12 October 2012
Q10009, doi:10.1029/2012GC004273
ISSN: 1525-2027

Magma degassing during the Plinian eruption of Novarupta, Alaska, 1912

H. M. Gonnermann
Department of Earth Science, Rice University, Houston, Texas 77005, USA (helge@rice.edu)

B. F. Houghton
Department of Geology and Geophysics, University of Hawai'i at Mānoa, Honolulu, Hawai'i 96822, USA

[1] We have modeled the nucleation and isothermal growth of bubbles in dacite from the 1912 Plinian eruption of Novarupta, Alaska. Bubble growth calculations account for the exsolution of H_2O and CO_2, beginning with bubble nucleation and ending when bubble sizes reproduced the observed size distribution of vesicles in Novarupta pumice clasts. Assuming classical nucleation theory, bubbles nucleated with a diameter of the order of 10^{-8} m and grew to sizes ranging from 10^{-6} m to greater than 10^{-3} m, the typical range of vesicle sizes found in Novarupta pumice. The smallest vesicles in Novarupta pumices are also the most abundant and bubbles with radii of 10^{-6} m to 10^{-5} m comprise almost 90% of the entire bubble population. We find that these bubbles must have nucleated and grown to their final size within a few 100 milliseconds. Despite these extremely fast growth rates, the pressures of exsolved volatiles contained within the bubbles remained high, up to about 10^7 Pa in excess of ambient pressure. Assuming a closed-system, the potential energy of these compressed volatiles was sufficient to cause magma fragmentation, even though only a fraction of the pre-eruptive volatiles had exsolved. Unless the matrix glasses of Novarupta pyroclasts retains a large fraction of pre-eruptive volatiles, the majority of magmatic volatiles (80–90%) was likely lost by open-system degassing between magma fragmentation and quenching.

Components: 13,400 words, 16 figures.

Keywords: Novarupta; bubble growth; bubble nucleation; explosive volcanism; magma degassing; volcanology.

Index Terms: 8414 Volcanology: Eruption mechanisms and flow emplacement; 8434 Volcanology: Magma migration and fragmentation; 8450 Volcanology: Planetary volcanism (5480, 6063, 8148).

Received 4 June 2012; **Revised** 29 August 2012; **Accepted** 5 September 2012; **Published** 12 October 2012.

Gonnermann, H. M., and B. F. Houghton (2012), Magma degassing during the Plinian eruption of Novarupta, Alaska, 1912, *Geochem. Geophys. Geosyst.*, *13*, Q10009, doi:10.1029/2012GC004273.

1. Introduction

[2] Styles of volcanic eruptions range from effusive to highly explosive. Because of their tremendous destructiveness, the latter pose a considerable threat to human life, economies and the environment. Because magma ascent is inaccessible to direct observation, eruptive products, pyroclasts in the case of explosive eruptions, provide the best direct record of eruptive conditions. In particular bubbles, which are preserved as vesicles within these pyroclasts, have been intensely studied with the objective of constraining

the conditions of magma ascent [e.g., *Sparks and Brazier*, 1982; *Mangan et al.*, 1993; *Klug and Cashman*, 1994; *Gardner et al.*, 1996; *Klug and Cashman*, 1996; *Mangan and Cashman*, 1996; *Hammer et al.*, 1999; *Blower et al.*, 2001a; *Polacci et al.*, 2001; *Blower et al.*, 2002; *Klug et al.*, 2002; *Polacci et al.*, 2003; *Gaonac'h et al.*, 2003, 2005; *Polacci*, 2005; *Polacci et al.*, 2006a, 2009; *Gurioli et al.*, 2005; *Polacci et al.*, 2006b; *Adams et al.*, 2006; *Lautze and Houghton*, 2007; *Piochi et al.*, 2008; *Giachetti et al.*, 2010; *Houghton et al.*, 2010; *Shea et al.*, 2010; *Giachetti et al.*, 2011; *Voltolini et al.*, 2011].

[3] Our study is focused on the eruption dynamics of Earth's most voluminous volcanic eruption of the 20th century, the Plinian eruption of Novarupta on June 6–8, 1912 [*Fierstein and Hildreth*, 1992; *Hildreth and Fierstein*, 2000]. We have constrained magma ascent conditions during Episode III of this eruption, by reconstructing the vesicle size distributions in pyroclasts from this episode, using accurate modeling of diffusive bubble growth during the exsolution of a mixed H_2O and CO_2 magmatic volatile phase [*Gonnermann and Manga*, 2005]. The 1912 eruption of Novarupta is widely recognized as an outstanding example of sustained Plinian explosive volcanism. It has been the subject of a century of intense study, resulting in a well-developed tephrostratigraphy [*Hildreth and Fierstein*, 2012, and references therein] and extensive textural analysis of air-fall deposits [*Adams et al.*, 2006], as well as thorough characterization of pre-eruptive magma storage conditions [*Hammer et al.*, 2002].

[4] The cause of explosive volcanism is the sudden release and rapid expansion of a volatile (gas) phase. During magma ascent the solubility of magmatic volatiles, to a large extent H_2O and CO_2, decreases as the confining pressure on the magma decreases. Consequently, the melt becomes supersaturated in volatiles, which results in the nucleation of bubbles by the exsolution of magmatic volatiles (gases). These bubbles will grow, due to diffusion of volatiles from the melt and the expansion of the already exsolved volatiles. During many explosive eruptions bubbles cannot grow as fast as pressure decreases in the surrounding melt by which they are transported to the surface. This is a consequence of the strong dependence of melt viscosity on the concentration of dissolved H_2O, which causes melt viscosity to increase upon H_2O exsolution. If the viscous timescale, which is approximately equal to the ratio of melt viscosity to the excess pressure inside bubbles, is larger than the time over which magma decompresses, then bubbles will not be able to grow fast enough to expand and equilibrate with the ambient pressure [*Lensky et al.*, 2004]. Consequently, the bubbles may be of considerably higher pressure than the surrounding melt.

[5] If this bubble overpressure exceeds a certain threshold [*McBirney and Murase*, 1970; *Alidibirov*, 1994; *Zhang*, 1999; *Spieler et al.*, 2004a; *Mueller et al.*, 2008], or if it causes sufficiently high rates of bubble growth [*Dingwell*, 1996; *Papale*, 1999], the viscoelastic rheology of the melt will cause it to fragment in a brittle manner. Fragmentation allows the pressurized volatiles to escape from their confinement and expand explosively in volume. This abrupt transition, from a continuous melt phase with suspended bubbles, to an explosively expanding gaseous flow with suspended magma fragments, called pyroclasts, is sustained for hours during Plinian eruptions. Pyroclasts are transported from their depth of fragmentation into the Earth's atmosphere, at velocities of hundreds of meters per second, by the rapidly expanding gases. When the pyroclasts settle out of this Plinian eruption column, they form aerially extensive pyroclastic air-fall deposits, with potentially severe environmental and societal impacts. Consequently, an understanding of the magmatic conditions leading up to and after magma fragmentation is of key importance in the study of explosive volcanism.

[6] A record of these conditions are the size distribution and number density of vesicles in the erupted pyroclasts. Number density is defined as number of vesicles per unit volume of solid matrix, presumably equivalent to the number of bubbles per unit volume of melt, prior to quenching. A question of fundamental importance is whether the ascending magma traverses a region of extreme decompression rates, of the order of 100 MPa s^{-1} [e.g., *Toramaru*, 1995, 1989, 2006]. It is unclear from experiments if $\sim$100 MPa s^{-1} is a necessary requirement to achieve the high bubble number densities observed in pyroclasts [*Mourtada-Bonnefoi and Laporte*, 2004; *Hamada et al.*, 2010; *Gardner and Ketcham*, 2011; *Gonde et al.*, 2011; *Nowak et al.*, 2011]. Relatively high rates of decompression are required to outpace the diffusion of dissolved volatiles into existing bubbles [e.g., *Sparks*, 1978; *Proussevitch et al.*, 1993; *Lyakhovsky et al.*, 1996; *Gardner et al.*, 1999; *Mourtada-Bonnefoi and Laporte*, 2002, 2004; *Lensky et al.*, 2004; *Gonnermann and Manga*, 2007], thereby driving the melt toward progressively increasing supersaturation and increasing rates of bubble nucleation. If at all, decompression

rates of ~100 MPa s^{-1} may only be plausible for a very short duration and within a short distance of the fragmentation depth, where viscosity may increases considerably over short distances, due to the exsolution of H_2O [e.g., *Woods*, 1995; *Papale*, 1999; *Mastin*, 2002; *Koyaguchi*, 2005; *Massol and Koyaguchi*, 2005; *Melnik et al.*, 2005]. For a given flow rate, and assuming Newtonian rheology, viscous resistance within the conduit requires that pressure decreases concurrently. This so-called frictional pressure loss can result in steep pressure gradients and high rates of decompression. If the latter outpaces the decrease in pressure within the expanding bubbles, the resulting difference in pressure between the interior of bubbles and the surrounding melt may exceed the overpressure at which magma will fragment [*Alidibirov*, 1994; *Dingwell*, 1996; *Papale*, 1999; *Zhang*, 1999; *Spieler et al.*, 2004a]. However, the buildup of overpressure may be modulated or balanced by the development of interconnected bubbles, amenable to gas loss from the erupting magma by permeable gas flow [*Burgisser and Gardner*, 2005; *Mueller et al.*, 2008; *Rust and Cashman*, 2011]. The objective of our study is to constrain the rates of magma decompression required to produce the vesicle size distributions in fall deposits from Episode III of the 1912 Novarupta eruption and to examine the relationship between bubble nucleation, growth and fragmentation.

[7] Section 2 gives a brief summary of the 1912 Novarupta eruption, its deposits and the samples modeled herein. In section 3 we provide a review of the quantitative description of vesicles in pyroclasts. It is followed by a discussion of bubble nucleation in section 4, the modeling thereof, as well as a brief synopsis of the role of surface tension in studies of bubble nucleation and the associated uncertainties. Section 5 presents the conceptual framework for a new approach to the modeling of vesicle size distributions, based on the modeling of diffusive bubble growth, described in section 6, followed by a step-by-step description of the model in section 7. Finally, section 8 presents a discussion of the model results, followed by conclusions in section 9.

2. Novarupta 1912

2.1. Eruption and Deposits

[8] The 1912 Novarupta eruption was the most voluminous eruption of the twentieth century. Because caldera collapse occurred 10 km from the vent, eruption deposits have been well preserved close to the vent. The explosive phase of the eruption began on 6 June, 1912 and lasted for 60 hours, with Plinian fall deposits and voluminous ignimbrites deposited during parts of the eruption [e.g., *Hildreth*, 1983; *Fierstein and Hildreth*, 1992; *Hildreth and Fierstein*, 2000, 2012]. Based on tephrostratigraphic relations and eyewitness accounts, it appears that there were two short breaks in the Plinian phase of the eruption, one on the morning of 7 June and the other in the evening of 8 June. Consequently, the explosive phase of the eruption is subdivided into three episodes, with inferred column heights of 26, 25, and 23 km respectively. Most of the ignimbrite was deposited during Episode I, whereas Episodes II and III predominantly formed Plinian fall deposits. After the explosive phase, two episodes of dome emplacement are designated as Episodes IV and V.

2.2. Pre-eruptive Volatile Content and Pressure

[9] The erupted magmas are rhyolite (77–78 wt% SiO_2), dacite (63–68 wt% SiO_2) and andesite (58–63 wt% SiO_2) [*Hildreth and Fierstein*, 2000]. Melt inclusions in quartz phenocrysts of the Novarupta rhyolite contain dissolved H_2O concentrations between 3.5 and 4.7 wt% and melt inclusions in plagioclase phenocrysts in dacite contain between 2.2 and 3.1 wt% H_2O [*Lowenstern*, 1993].

[10] The CO_2 content of both rhyolites and dacites is less than 50 ppm [*Lowenstern*, 1993; *Wallace*, 2005]. We focus our study on the 1912 Novarupta dacite from Episode III. Using experimental phase relations at H_2O + CO_2 fluid saturation, *Hammer et al.* [2002] determined a H_2O saturation pressure of approximately 50 MPa at 850°C at a total pressure of 50–150 MPa for the dacite. However, concentrations of less than 50 ppm CO_2 in melt inclusions, suggests relatively limited H_2O undersaturation, caused by the presence of a CO_2-rich vapor phase [*Blundy et al.*, 2010]. An alternate possibility suggested by *Hammer et al.* [2002] is H_2O undersaturation, due to a lack of H_2O.

[11] The presence of CO_2 can modulate the nucleation rate of bubbles [*Mourtada-Bonnefoi and Laporte*, 2002; *Yamada et al.*, 2005; *Larsen*, 2008] and affect eruption dynamics [*Papale and Polacci*, 1999], especially at shallow depths [*Burgisser et al.*, 2008]. In our model we, therefore, focus on the dacite end-member suggested by *Hammer et al.* [2002], which equilibrated at 850°C, a H_2O saturation pressure of 50 MPa, and a vapor phase with 10 mole % of CO_2.

2.3. Existing Textural Analyses of Novarupta Plinian Fall Pumices

[12] *Adams et al.* [2006] carried out a detailed textural study of the 1912 Novarupta Plinian fall deposits. They sampled and texturally characterized dacite pumice clasts from Episodes II and III and the modeling described herein builds upon this analysis. *Adams et al.* [2006] obtained vesicle size distributions through a two-dimensional analysis of Scanning Electron Microscope (SEM) images from polished thin sections for a subset of pumice clasts of individual sample suites. Number densities of vesicles were calculated for binned vesicle diameters thus obtained and converted from two-dimensional to three-dimensional number densities using the method of *Sahagian and Proussevitch* [1998]. This methodology may result in some bias, due to the inherent spherical assumption. However, given the present limitation associated with the estimation of VSDs from three-dimensional Computed Tomography (CT) scans, the method employed by *Adams et al.* [2006] provides the most robust estimate of VSDs for the Novarupta samples [*Giachetti et al.*, 2011].

2.4. Qualitative Interpretation of Novarupta Plinian Fall Pumices

[13] Similarities in bubble number density, N_m, and vesicle size distributions, $n(a)$, of Novarupta pyroclasts have been interpreted to signify similar magma ascent conditions [*Adams et al.*, 2006]. Near-unimodal vesicle volume fractions, with a relatively invariant mode throughout episodes II and III, are thought to indicate that magma ascent conditions remained relatively constant, with bubble nucleation and growth occurring over a short time interval [*Toramaru*, 1989, 1990; *Lyakhovsky et al.*, 1996; *Gardner et al.*, 1999; *Adams et al.*, 2006]. At the same time, the abundance of small vesicles are thought to indicate continuous nucleation until the late stages of magma ascent [*Adams et al.*, 2006], presumably associated with homogenous nucleation at large supersaturations [*Hurwitz and Navon*, 1994; *Gardner et al.*, 1999; *Mourtada-Bonnefoi and Laporte*, 1999; *Mangan and Sisson*, 2000]. Because the distribution $n(a)$ is considerably more skewed toward small vesicles than would be expected for steady state nucleation and growth [*Lyakhovsky et al.*, 1996; *Blower et al.*, 2001b; *Klug et al.*, 2002; *Adams et al.*, 2006], the bubble nucleation rate may have increased with time, perhaps modulated by bubble coalescence [*Gaonac'h et al.*, 1996; *Simakin et al.*, 1999; *Mangan et al.*, 2004].

2.5. Modeled Samples

[14] We model three Plinian dacite fall clasts from Episode III, Unit G, sampling site 94-Z, sample No. 22 [*Adams et al.*, 2006]. They are named 94-Z-22-28, 94-Z-22-24 and 94-Z-22-8 and represent high, modal and low-density clasts with a vesicularity of 75.2%, 63.5% and 51.7%, respectively [see *Adams et al.*, 2006, Figure 8]. Bubble number density ranges between $\sim 10^{14}$ and $\sim 10^{15}$ m^{-3}, with median vesicle diameter between 45 and 74 μm for vesicles ranging in size between 4 and 1989 μm (see Table 1 of *Adams et al.* [2006] for details). Various stages of bubble coalescence are evident in the samples and the walls of coalesced bubbles are approximately 1–3 μm in thickness, similar to Plinian dacites and rhyolites elsewhere [*Klug and Cashman*, 1996; *Klug et al.*, 2002].

[15] Novarupta dacites contain phenocrysts (predominatly plagioclase with minor clinopyroxene and magnetite) [*Hildreth*, 1983] and a few plagioclase microlites [*Adams et al.*, 2006]. Because plagioclase is not amenable to nucleation and because the size and number density of bubbles is not significantly higher around phenocrysts, heterogenous bubble nucleation associated with crystals is not likely to have been of importance at Novarupta [e.g., *Hurwitz and Navon*, 1994; *Gardner and Denis*, 2004; *Mourtada-Bonnefoi and Laporte*, 2004; *Gardner*, 2007a; *Larsen*, 2008].

3. Vesicle Size Distributions in Pyroclasts

[16] Vesicle size distributions (VSDs) in pyroclasts are frequently used to infer conditions of syneruptive magma vesiculation, that is bubble nucleation, growth and coalescence. VSDs represent one example of what is known generically as a population distribution. The standard approach to quantitative studies of population distributions is the population balance equation (PBE), which describes the temporal change in a population distribution due to the addition (*birth*), change in size (*growth*) and loss (*death*) of individual members of the distribution. In our case, *birth* denotes bubble nucleation, as a consequence of volatile supersaturation of the melt. *Growth* refers to bubble growth as a consequence of decreasing pressure and exsolution of volatiles. It could also include a decrease in bubble size, due to open-system gas loss, which is not considered explicitly herein. Last, *death* refers to bubble coalescence.

[17] Consequently, a quantitative interpretation of VSDs requires the estimation of nucleation rate $J(t)$, growth rate $G(a, t)$ and coalescence rate $H(a, t)$, either by forward or by inverse modeling. However, one of the challenges lies in the difficulty of solving the population balance equation [*Ramkrishna*, 2000]. Much of this difficulty arises due to the coalescence term, which, despite recent progress [e.g., *Larsen and Gardner*, 2000; *Burgisser and Gardner*, 2005; *Gardner*, 2007b; *Bai et al.*, 2008; *Gonde et al.*, 2011], remains to a large extent insufficiently constrained as an a-priori model parameter [e.g., *Gaonac'h et al.*, 1996; *Klug and Cashman*, 1996; *Herd and Pinkerton*, 1997; *Blower et al.*, 2002; *Gaonac'h et al.*, 2003, 2005; *Lovejoy et al.*, 2004]. We therefore do not model bubble coalescence. After providing a brief review on the quantitative descriptions of VSDs in this section, we discuss bubble nucleation and growth in subsequent sections.

3.1. Number Density

[18] The total number of vesicles in a sample is given by

$$n_{\mathrm{tot}} = \sum n_i, \tag{1}$$

where n_i is the number of vesicles per size class i, which frequently is defined in terms of vesicle radius or volume. If, for example, a denotes vesicle radius, then there are n_i vesicles of radius $a_i < a \leq (a_{i+1})$. Because of the wide range in vesicle sizes found in pyroclasts, the value of a_i is often taken to increase geometrically by a factor of δ, so that $\log a_i = i\delta$. VSDs in Novarupta pyroclasts have been characterized with $\delta = 0.1$ [e.g., *Adams et al.*, 2006].

[19] The total number of vesicles per unit volume of matrix, called the vesicle number density, is given by

$$N_{\mathrm{m}} = \frac{n_{\mathrm{tot}}}{v_m}, \tag{2}$$

where v_m is the volume of matrix, which usually is comprised of glass or glass plus microlites. Here we define N_m as the number of vesicles per unit volume of glass matrix. Although bubbles may continue growing during the time interval between magma fragmentation and pyroclast quenching [*Thomas et al.*, 1994; *Gardner et al.*, 1996], especially in large clasts or where cooling rate is slow, conventionally it is thought that N_m is a reasonable approximation to the bubble number density (BND), the number of bubbles per unit volume melt prior to quenching of the pyroclast [e.g., *Toramaru*, 2006]. Therefore, we shall use the terms vesicle number density and bubble number density interchangeably herein. N_m provides a time-integrated record of bubble nucleation, albeit potentially modulated by bubble coalescence. It is found the N_m varies considerably among pyroclasts from various eruptions [*Toramaru*, 2006; *Rust and Cashman*, 2011].

[20] The vesicle number density, $n(a_i)$, and the exceedance density, $N(a_i)$, are two frequently used representations of VSDs. They are defined, respectively, as the number of vesicles within a given size interval per volume of solid matrix

$$n(a_i) = \frac{1}{v_m}\frac{n_i}{(a_{i+1} - a_i)}, \tag{3}$$

the number of vesicles per volume of matrix that are greater than or equal to size a_i

$$N(a_i) = \sum_i^{\infty} n(a_i). \tag{4}$$

3.2. Volume Fraction Density

[21] Vesicle size distributions in pumice are frequently logarithmic [*Proussevitch et al.*, 2007] and detailed population characteristics, such as multiple modes, may not be easily recognizable on logarithmically plotted distribution densities $n(a_i)$ or $N(a_i)$. Vesicle volume fractions, $\phi(a_i)$, also called vesicle volume distributions (VVDs), are not logarithmically distributed, because of the decrease in volume for small vesicle sizes. $\phi(a_i)$ is defined as the volume of vesicles within a given size range, divided by the total volume of vesicles in the sample,

$$\phi(a_i) = \sum_{a=a_i}^{a_{i+1}} n(a)a^3 \Big/ \sum_{a=0}^{\infty} n(a)a^3, \tag{5}$$

and provides a useful complement to $n(a_i)$ and $N(a_i)$ [*Sparks and Brazier*, 1982; *Klug and Cashman*, 1994; *Mangan and Cashman*, 1996; *Herd and Pinkerton*, 1997; *Klug et al.*, 2002; *Shea et al.*, 2010].

4. Bubble Nucleation

4.1. Classical Nucleation Theory

[22] Based on classical nucleation theory [*Hirth et al.*, 1970; *Sparks*, 1978; *Hurwitz and Navon*, 1994; *Mangan and Sisson*, 2005], the rate of bubble nucleation, J, is thought to depend on the volatile supersaturation of the melt as

$$J = C\exp\left(-\frac{16\pi\sigma^3}{3k_BT\Delta P_s^2}\psi\right). \tag{6}$$

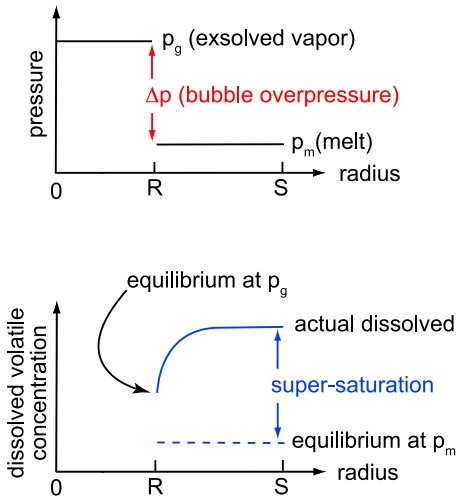

Figure 1. Schematic diagram illustrating supersaturation pressure, ΔP_s, the difference between the pressure at which the melt would be saturated (in equilibrium) with the dissolved volatiles, p_{sat}, and the actual pressure, p_m.

Here σ is the surface tension between the melt and the exsolved magmatic volatiles, $k_B = 1.3805 \times 10^{-23}$ J/K is the Boltzmann constant and T is the absolute temperature. $0 \leq \psi \leq 1$ is a geometrical factor that accounts for the presence of impurities (e.g., crystals), which lower the interfacial energy associated with the formation of a stable bubble nucleus [e.g., *Hurwitz and Navon*, 1994; *Gardner and Denis*, 2004; *Mourtada-Bonnefoi and Laporte*, 2004; *Gardner*, 2007a; *Larsen*, 2008]. C is a pre-exponential factor and ΔP_s is the supersaturation pressure given by

$$\Delta P_s = p_{\text{sat}} - p_m, \tag{7}$$

where p_m is the pressure of the melt and p_{sat} is the pressure at which melt would be saturated with the actual concentration of dissolved volatiles, assuming equilibrium conditions (Figure 1). For silicate melts, C is usually given as [*Hirth et al.*, 1970; *Sparks*, 1978; *Hurwitz and Navon*, 1994; *Mangan and Sisson*, 2005]

$$C = \frac{2n_0^2 V_m D}{a_0}\sqrt{\frac{\sigma}{k_B T}}. \tag{8}$$

Here n_0 is the number of dissolved volatile molecules per volume of liquid (melt), V_m is the volume of a volatile molecule, D is the diffusivity of the volatile species in the liquid (melt) and $a_0 \approx n_0^{-1/3}$ is the mean distance between dissolved volatile molecules. Note that $n_o = (N_A X \rho_m / M)$, where $N_A = 6.02 \times 10^{23}$ is Avogadro's number, ρ_m is the melt density, M is the molar mass of the volatile species, and X is the mass fraction of dissolved volatiles.

[23] The presence of impurities, such as crystals, with lower interfacial energy between bubble (i.e., vapor) and solid (i.e., crystal) than the interfacial energy between vapor and liquid (i.e., melt), decreases the Gibbs free energy of a stable bubble nucleus. Consequently, higher nucleation rates can be achieved at a given supersaturation. Nucleation in the presence of such nucleation sites is called heterogeneous nucleation, as opposed to homogeneous nucleation. All else being equal, $\Delta P_{s,\text{hetero}} < \Delta P_{s,\text{homo}}$ and within the context of classical nucleation theory is a consequence of $\psi < 1$. The theoretical value of ψ is determined by the contact angle θ between nucleation sites and exsolved vapor phase (Figure 2)

$$\psi = \frac{(2 - \cos\theta)(1 + \cos\theta)^2}{4}. \tag{9}$$

The wetting angle is controlled by the relative values of the interfacial (surface) tensions: vapor-liquid (σ_{LB}), vapor-solid (σ_{SB}), and solid-liquid (σ_{SL}). It is defined as

$$\cos\theta = \frac{\sigma_{\text{SB}} - \sigma_{\text{SL}}}{\sigma_{\text{LB}}}. \tag{10}$$

For $\theta < 90°$ the bubble is poorly wetting, as opposed to for $\theta > 90°$. For $\theta = 0°$ the value of $\psi = 1$ and the presence of crystals has no effect on nucleation. ψ also depends on the shape of the nucleation substrate, where Equation (9) corresponds to the case of a planar substrate. Relative to a planar surface, the nucleation efficiency will be enhanced on a concave substrate, but reduced on a convex substrate [*Cluzel et al.*, 2008, and references therein].

[24] In many natural and artificial systems nucleation proceeds at significantly higher rates than would be predicted by classical nucleation theory. A number of explanations have been proposed to explain this discrepancy, including the presence of submicroscopic impurities or inhomogeneities to reduce the energy barrier for nucleation [e.g., *Lubetkin*, 2003]. To what extent bubble nucleation in erupting

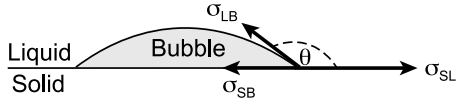

Figure 2. Schematic diagram illustrating the definition of contact angle, θ, and interfacial tension between solid and bubble, σ_{SB}, liquid and bubble, σ_{LB}, as well as solid and liquid, σ_{SL}. If the volatiles within the bubble are more wetting to the solid (crystal) than the liquid (melt), then $\theta > 90°$.

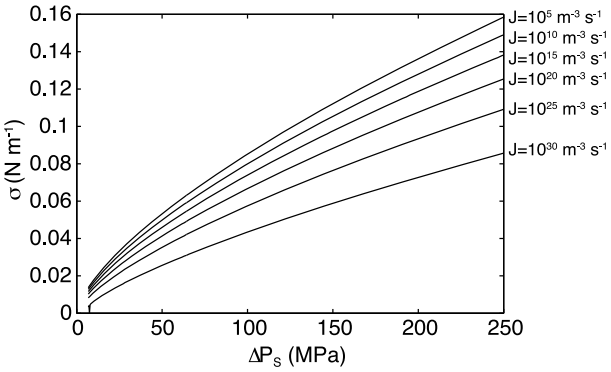

Figure 3. Contours of predicted bubble nucleation rates (black lines) for Novarupta dacite at 850°C, for different supersaturation pressures, ΔP_s, as well as corresponding dissolved H_2O content and H_2O diffusivity [*Zhang and Ni*, 2010] and surface tension, σ.

magmas occurs at higher rates than would be predicted from classical nucleation theory, as seems to be the case for many other nucleation processes, is an important question [e.g., *Mourtada-Bonnefoi and Laporte*, 2004]. Thus, empirical values of surface tension for natural silicate melts may perhaps constitute an *effective* surface tension

$$\sigma_e = \sigma\, \psi^{1/3}, \tag{11}$$

with ψ accounting not only for the presence of crystals, but any other effect that reduces Gibbs free energy of a stable bubble nucleus.

4.2. Bubble Nucleation During Magma Ascent

[25] During rapid magma ascent and decompression, the melt may become increasingly supersaturated, if volatiles cannot diffuse fast enough from the melt into bubbles [e.g., *Lensky et al.*, 2004]. However, even if diffusion is fast enough, the melt may become supersaturated if bubbles cannot grow fast enough, relative to the rate of magma ascent and decompression. In this case the pressure of exsolved volatiles within bubbles remains high. The ability of volatiles to diffuse and exsolve into bubbles depends on the concentration of dissolved volatiles at the melt-vapor interface, which in turn depends on the pressure of the exsolved volatiles within bubbles. Therefore, if bubbles cannot grow fast enough, the resultant overpressure prevents volatile exsolution, resulting in supersaturation [e.g., *Gonnermann and Manga*, 2007].

[26] Classical nucleation theory predicts a continuous and steep increase in nucleation rate as ΔP_s increases, with nucleation rates of up to $\sim 10^{30}$ bubbles m^{-3} s^{-1} for values of $\Delta P_s \sim 100$ MPa (e.g., Figure 3) [*Mangan and Sisson*, 2005]. To what extent continuous nucleation is substantiated by experiments, where in some cases it appears that nucleation occurs as a discrete event, is unclear [e.g., *Gardner et al.*, 1999; *Mourtada-Bonnefoi and Laporte*, 1999, 2004; *Gardner and Ketcham*, 2011]. Models of continuous nucleation predict a steep increase in nucleation rate within a very short time interval [e.g., *Toramaru*, 1989, 1995], perhaps experimentally indistinguishable from a discrete event.

[27] During the steep increase in nucleation rate associated with rapid decompression and increasing supersaturation, the spatial density of bubbles will reach a threshold where all of the melt begins to be affected by volatile diffusion into bubbles. Because J is so strongly dependent on supersaturation, it will rapidly drop to zero once this threshold is reached [e.g., *Toramaru*, 1989, 1995; *Mourtada-Bonnefoi and Laporte*, 2002]. How soon after the onset of nucleation this threshold is reached depends on the relative rates of diffusion and decompression. The former scales as the ratio of volatile diffusivity to the square of the thickness of melt between individual bubbles, which decreases as the number and size of bubbles increases. Consequently, the rates of bubble growth assert a strong control on the time interval over which bubbles can nucleate.

[28] As depicted in Figure 4, the entire process may be envisaged by a volume of magma that consists of fully saturated melt, bubbles and surrounding diffusion envelopes [*Kedrinskiy*, 2009]. The threshold for the cessation of bubble nucleation can be viewed as the time, τ_n, at which the entire melt volume is encompassed by diffusion envelopes [*Toramaru*, 1989, 1995; *Kedrinskiy*, 2009]. Within this conceptual framework, and neglecting bubble coalescence,

$$N_m = \int_0^{\tau_n} J\, dt_n, \tag{12}$$

where t_n is the time since the onset of nucleation.

4.3. The Moments of the Bubble Size Distribution

[29] One approach to modeling N_m has been to solve the equation of motion about moments of the bubble size distribution, assuming that there is no coalescence or breakage of bubbles [e.g., *Randolph and Larson*, 1971; *Toramaru*, 1989, 1995]. This

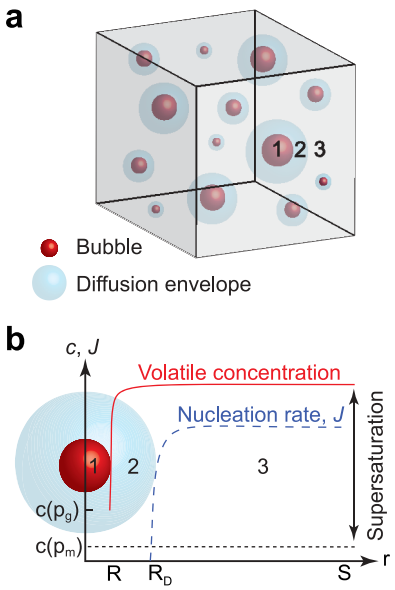

Figure 4. (a) Schematic representation of the proposed bubble nucleation and growth model [e.g., *Kedrinskiy*, 2009, Figure 10]. (1) represents the bubble; (2) represents the diffusion envelope that is the part of the melt where volatile concentrations and correspondingly nucleation rates are low; and (3) is the nucleation region. (b) Schematic graph of volatile concentration in the melt, c, as a function of radial distance, r. The concentration, $c(p_g)$, at the melt-vapor interface ($r = R$) is dependent on the pressure of the exsolved volatiles (gas)inside the bubble, p_g. The difference between the actual volatile concentration (solid red) and the equilibrium saturation concentration, $c(p_m)$, at ambient pressure, p_m, is the supersaturation. Nucleation rate (long-dashed blue), J, is negligible inside the diffusion envelope of radius $r = R_D$. The radius of the melt shell associated with a given bubble is denoted as $r = S$ and nucleation ceases when the radius of the diffusion envelope approaches a value of $R_D \rightarrow S$.

method has been employed to assess magma decompression rates and we summarize it here to provide the necessary background for the subsequent discussion on modeling of VSDs via diffusive bubble growth.

[30] The zeroth moment, M_0 of the BSD equals N_m and is calculated as

$$\frac{M_0}{dt} = \frac{N_m}{dt} = J. \tag{13}$$

The first moment, M_1, is given by

$$\frac{M_1}{dt} = GM_0, \tag{14}$$

where G is the growth rate of a bubble with mean radius $\bar{R} = M_1/M_0$. Higher order moments are calculated from

$$\frac{M_j}{dt} = jGM_{j-1}. \tag{15}$$

[31] The zeroth and first order moments have been the primary focus of previous studies [*Toramaru*, 1989, 1995, 2006]. In addition to Equations (6), (13) and (15), the zeroth and first order moments require an equation for the average bubble growth rate $G = d\bar{R}/dt$. Bubble growth is governed by mass conservation of volatiles and momentum balance of the melt-fluid interface. The latter, assuming constant melt viscosity, η, and a spherical bubble geometry, is given by

$$\frac{d\bar{R}}{dt} = \frac{\bar{R}}{4\eta}\left(p_g - p_m - \frac{2\sigma}{\bar{R}}\right), \tag{16}$$

where p_g is the gas pressure inside bubbles and p_m the pressure in the surrounding melt.

[32] Typically, p_m decreases at some prescribed rate, dp_m/dt, whereas p_g is calculated from conservation of mass

$$\frac{d}{dt}\left(p_g\bar{R}^3\right) = 4\frac{BT}{m}\bar{R}^2\rho_m D\left(\frac{\partial c_w}{\partial r}\right)_{r=\bar{R}}. \tag{17}$$

Here B is the universal gas constant, T is absolute temperature, m is the molar mass of the volatile species, ρ_m is the density of the melt, r is the radial coordinate with $r = 0$ at the bubble center, and c_w is the concentration of dissolved H_2O. The diffusive flux of volatiles from the melt into the bubble depends on the concentration gradient at the bubble wall, which can be obtained from the mean field approximation [*Toramaru*, 1989]

$$\left(\frac{\partial c_w}{\partial r}\right)_{r=\bar{R}} \approx \frac{c_{w,0} - c_{w,p_g}}{\bar{R}}. \tag{18}$$

Here $c_{w,0}$ is the initial volatile content and c_{w,p_g} is the equilibrium volatile content at pressure p_g, obtained from a suitable solubility formulation.

4.4. The Role of Surface Tension, σ

[33] The advantage of solving Equations (13)–(15), together with Equations (16) and (17), lies in the efficiency of the mean field approximation (Equation (18)), albeit at the cost of potential inaccuracies. It also requires explicit calculation of J in Equation (13), which requires that σ is known. However, because of the exceedingly strong dependence

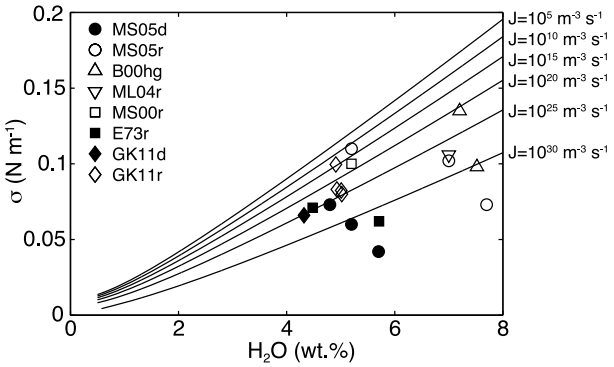

Figure 5. Experimentally determined values of surface tension, σ, for rhyolitic (open symbols) and dacitic (filled symbols) melts at different dissolved H_2O contents. Also shown are contours of predicted bubble nucleation rates (black lines) for a Novarupta dacite at 850°C, different dissolved H_2O content and H_2O diffusivity calculated from the formulation of *Zhang and Ni* [2010]. Most experimentally determined values of σ are at high water content and, under the assumption of classical nucleation theory, would predict very high nucleation rates, *J*. Moreover, uncertainties in σ by only a few percent result in predictions of *J* that differ by several orders in magnitude. Experimental values are by *Mangan and Sisson* [2005] (rhyolite: MS05r, dacite: MS05d), *Bagdassarov et al.* [2000] (haplogranite: B00hg), *Mourtada-Bonnefoi and Laporte* [2004] (rhyolite: ML04r), *Mangan and Sisson* [2000] (rhyolite: MS00r), *Epel'baum et al.* [1973] (rhyolite: E73r) and *Gardner and Ketcham* [2011] (rhyolite: GK11r, dacite: GK11d).

of *J* on σ (Equation (6)), relatively modest uncertainties in σ can significantly affect model predictions (Figure 3).

[34] That there is considerable uncertainty in σ is shown in Figure 5, which includes a compilation of the empirical values of σ for rhyolitic and dacitic melts; note that these are determined almost exclusively at water contents above 4 weight percent (wt.%). Because of the tradeoff between ΔP_s and σ (Figure 3), uncertainties in σ, especially at low H_2O, will translate into significant uncertainties in ΔP_s and in predicted decompression rates via the method of moments. This problem may be further exacerbated by the limitations associated with classical nucleation theory itself, which for many different nucleation processes tends to under-predict nucleation rates [e.g., *Lubetkin*, 2003].

[35] In contrast to bubble nucleation, bubble growth is relatively insensitive to σ, if bubbles are of radius $>10^{-6}$ m (Figure 6), the lower bound for vesicles preserved in many pyroclasts, including those from Novarupta [*Adams et al.*, 2006]. This fact provides the main motivation for our methodology of estimating *J* and dp_m/dt indirectly from calculations of diffusive bubble growth, which furthermore do not employ the mean field approximation.

5. Conceptual Framework for Modeling Bubble Size Distributions

[36] The monotonic or near-monotonic increase in vesicle abundance with decreasing size of the Novarupta VSDs [*Adams et al.*, 2006] can be interpreted to be produced during a period of continuous bubble nucleation and growth, during which supersaturation and, hence, *J* continually increased [*Toramaru*, 1989, 1995; *Massol and Koyaguchi*, 2005; *Nowak et al.*, 2011]. Within this conceptual framework, the smaller a bubble, the younger it is [e.g., *Yamada et al.*, 2008] and its growth time, τ, can be obtained from diffusive bubble-growth simulations, where $\tau(a)$ is the time for each of $n(a)$ vesicles to grow to size *a* after nucleation. We shall assume that bubble growth ends at time t_f, and that this time is the same for all bubbles. Therefore, a bubble nucleated time $t = t_f - \tau_a$. It is thus possible to transform $N(a)$ to $N(t)$ and to estimate the nucleation rate as

$$J(t) = \frac{dN(t)}{dt}. \tag{19}$$

[37] Assuming that the maximum nucleation rate occurs when the maximum degree of supersaturation

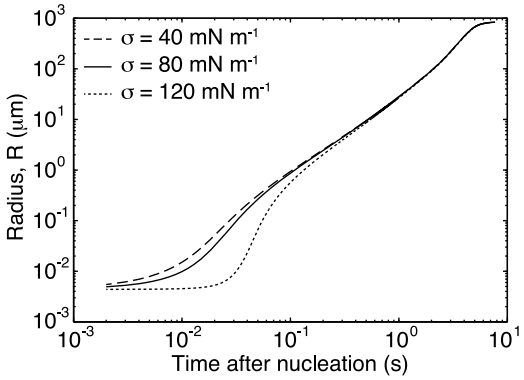

Figure 6. Modeled bubble radius, *R*, as a function of time after nucleation for constant values of surface tension, σ. Initial dissolved H_2O and CO_2 are 2.62 wt.% and 34 ppm, respectively. Melt composition is Novarupta dacite, temperature is 850°C, diffusivity is calculated using the formulation of *Zhang and Ni* [2010], solubility is calculated using the formulation of *Liu et al.* [2005], and viscosity using the formulation of *Hui and Zhang* [2007].

is reached, the pre-eruptive pressure of magma storage, P_{ch}, provides an upper bound on the supersaturation pressure, ΔP_s. Together with the maximum nucleation rates and Equation (6) it is thus possible to obtain a lower bound on σ_e. Assuming a constant σ_e permits the calculation of $\Delta P_s(t)$ from $J(t)$ and subsequently a minimum decompression rate

$$\frac{dp_m}{dt} = \frac{d}{dt}[\Delta P_s(t)]. \quad (20)$$

6. Diffusive Bubble Growth Modeling

6.1. Spatial Distribution of Bubbles

[38] Conceptually we assume that the vesicle size distribution, $n(a)$, is the consequence of bubbles nucleating throughout the time interval $0 \le t \le \tau_n$ and at random locations within the supersaturated melt that is not encompassed by diffusion envelopes (Figure 4). Once a bubble is nucleated it starts growing and its time of nucleation, $\tau_f - \tau_a$, and final bubble radius, $R = a$, are inversely correlated. That is, the oldest bubbles have the largest radii.

[39] For simplicity, we assume that the final distribution, $n(R) = n(a)$, approximates a smoothly varying concentration of dissolved volatiles throughout the melt. Given the spherical approximation of bubble growth [e.g., *Amon and Denson*, 1984; *Arefmanesh and Advani*, 1991; *Proussevitch et al.*, 1993], this corresponds to the condition that the volatile concentration at the outer radius of the melt shell, $c_{r=S}$, has the same value for all bubbles. The resultant spatial distribution of bubble cells would be space-filling and similar to an Apollonian packing geometry [*Borkovec et al.*, 1994; *Blower et al.*, 2002].

6.2. Bubble Nucleus

[40] We assume that the size of the critical bubble nucleus can be derived from the Laplace relation, which describes the mechanical equilibrium condition for a bubble

$$p_g - p_m = \frac{2\sigma}{R}. \quad (21)$$

The critical bubble radius, R_c, that satisfies Equation (21) is given by [e.g., *Proussevitch et al.*, 1993]

$$R_c = \frac{2\sigma}{\Delta P_s}. \quad (22)$$

If $R < R_c$ the bubble will shrink and disappear. To assure bubble growth, the initial bubble therefore has to satisfy the condition $R > R_c$ [e.g., *Proussevitch et al.*, 1993] and we use an initial bubble radius of $R = (1 + \gamma)\, R_c$, with $\gamma = 10^{-2}$.

6.3. Diffusive Bubble Growth

[41] Bubble growth is a consequence of magma decompression, due to a decrease in ambient pressure, p_m. This decrease in ambient pressure causes volume expansion of the already exsolved volatiles and the further diffusion of volatiles from the melt into existing bubbles. Here we consider both H_2O and CO_2 as the exsolving volatile species. The solubilities of H_2O and CO_2, denoted as s_w and s_c, respectively, are based on the formulation by *Liu et al.* [2005] and represent a reasonable approximation for joint H_2O-CO_2 solubilities in dacite melts [*Zhang et al.*, 2007]. s_w and s_c depend on temperature and their partial pressure within the coexisting gas phase, $(1 - x_c)\, p_g$ and $x_c\, p_g$, respectively. Here x_c is the mole fraction of exsolved CO_2 within the bubble.

6.3.1. Volatile Exsolution

[42] The mass flux of each volatile species into a bubble is determined by the concentration gradient in the melt at $r = R$, the melt-gas interface

$$q_i = D_i \left(\frac{\partial c_i}{\partial r}\right)_{r=R}. \quad (23)$$

Here c_i is the concentration of volatile species i ($i = w$ for H_2O or $i = c$ for CO_2). D_i is the diffusivity of the given species within the melt, based on Equations 20 and 41 of *Zhang and Ni* [2010] for H_2O and CO_2, respectively. The concentration of dissolved H_2O and CO_2 at $r = R$ are assumed to be equilibrium solubilities at pressure p_g and vapor phase composition x_c [*Liu et al.*, 2005]. As indicated by Equation (22), newly nucleated bubbles are under considerable internal pressure ($p_g - p_m \sim 10^7$ Pa), because of the Laplace pressure, $2\sigma/R$ [*Toramaru*, 1989, 1995]. During the early stages of bubble growth, the associated decrease in Laplace pressure asserts a strong influence on volatile exsolution, given that s_w and s_c are strongly pressure dependent [*Liu et al.*, 2005]. This potentially rapid change in s_w and s_c results in steep concentration gradients and large fluxes, q_i, of exsolving volatiles.

6.3.2. Volatile Diffusion

[43] The mass flux of exsolving volatiles is calculated from a diffusion model for volatiles within the melt surrounding each bubble. We employ the cell model for bubble growth [e.g., *Amon and Denson*,

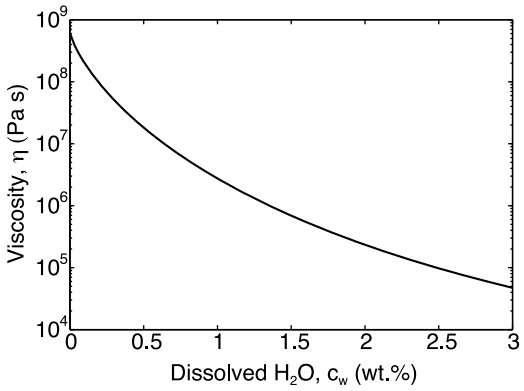

Figure 7. Viscosity, η, as a function of dissolved water, c_w, for Novarupta dacite, based on the formulation of *Hui and Zhang* [2007] at a temperature of 850°C.

1984; *Arefmanesh and Advani*, 1991; *Proussevitch et al.*, 1993], wherein bubbles are assumed to be spatially distributed such that each bubble can be approximated as a sphere surrounded by a spherical melt shell of thickness $S - R$. Because of the spherical symmetry inherent in this approximation, volatile diffusion simplifies to

$$\frac{\partial c_i}{\partial t} + v_r \frac{\partial c_i}{\partial r} = \frac{1}{r^2} \frac{\partial c_i}{\partial r} \left(D_i r^2 \frac{\partial c_i}{\partial r} \right), \tag{24}$$

where $v_r = dR/dt$ is the radial velocity of melt at $r = R$. Equation (24) is solved using an implicit finite difference scheme in a Lagrangian frame of reference and with a non-uniform grid. The latter assures that concentration gradients at the melt-vapor interface are accurately resolved [*Arefmanesh and Advani*, 1991; *Proussevitch et al.*, 1993]. The boundary condition at $r = S$ is

$$\left(\frac{\partial c_i}{\partial r} \right)_{r=S} = 0, \tag{25}$$

and as mentioned previously,

$$(c_i)_{r=R} = s_i(p_g, x_c). \tag{26}$$

6.3.3. Mass Conservation

[44] Mass conservation of volatiles requires that

$$\frac{d}{dt} \left(\rho_g R^3 \right) = 4R^2 \rho_m \sum_i q_i, \tag{27}$$

where the density of the exsolved gas phase, ρ_g, depends on p_g via an equation of state [*Kerrick and Jacobs*, 1981] and melt density, $\rho_m = 2400$ kg m^{-3}, [*Spera*, [2000] is approximated as constant. We assume that each bubble grows as a closed system. In other words, no gas is lost from the bubble. This approximation is valid if the timescale for bubble growth is much shorter than the characteristic timescale for permeable flow through interconnected bubbles. We provide an assessment of this assumption in section 8.5.

6.3.4. Momentum Balance

[45] Bubbles grow as a consequence of volatile flux into bubbles and volume expansion of the already exsolved volatiles. The balance between volume expansion and additional exsolution of volatiles determines how much p_g and, hence, ρ_g decrease. Bubble growth is resisted by viscous and capillary stresses, which are balanced by the pressure difference between the gas mixture inside the bubble and the surrounding melt

$$p_g(t) - p_m(t) = \frac{2\sigma}{R} + 4\eta_e \frac{1}{R} \frac{dR}{dt}. \tag{28}$$

Here η_e is the effective viscosity accounting for the radially variable H_2O-dependent viscosity (Figure 7) [*Lensky et al.*, 2001; *Hui and Zhang*, 2007] and dR/dt is the radial velocity of the melt-vapor interface. The pressure in the surrounding melt, p_m, is a boundary condition and may be time-dependent.

6.3.5. Solution Method

[46] The coupled Equations (24)–(28) are solved using a similar formulation as described by *Arefmanesh and Advani* [1991] and by *Proussevitch et al.* [1993]. However, in our case Equation (24) has to be solved separately for H_2O and CO_2, but with concentration boundary conditions, that couple both diffusion calculations. At each time step a consistent solution for Equations (24)–(28) is obtained through nonlinear minimization of the difference between gas volume predicted by Equations (27) and (28). Because we model bubble growth over a range of bubble sizes spanning up to 6 orders of magnitude, the nonlinear grid-spacing parameter for Equation (24), discussed in detail by *Proussevitch et al.* [1993] and by *Chouet et al.* [2006], is optimized to maintain good mass balance of H_2O and CO_2 throughout the calculation.

7. Modeling the Bubble Size Distribution

[47] We focused our study on the three aforementioned clasts from Episode III of the 1912 Novarupta eruption (section 2.5), because they represent a range

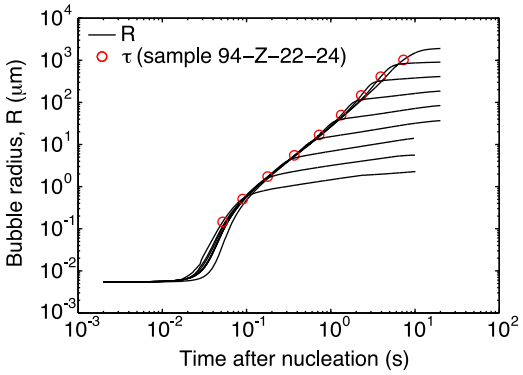

Figure 8. Modeled bubble radius, R, as a function of time after bubble nucleation, for bubbles with different-size diffusion envelopes ranging from $v_m = 1$ μm (smallest R) to $v_m = 10^8$ μm (largest R) in factors of 10.

in clast vesicularity and afford the opportunity to investigate potential differences in the vesiculation process within a sample.

7.1. Initial Conditions

[48] Initial conditions were based on the experimental work by *Hammer et al.* [2002], who determined pre-eruptive volatile saturation and pressure using mineral phase relations. They obtained a pre-eruptive H_2O saturation pressure for Novarupta dacite of $p_{H_2O} = 50$ MPa at a temperature of 850°C. Natural mineral and melt compositions were also reproduced under saturation conditions with a mixed $H_2O + CO_2$ fluid for the same p_{H_2O}, if the fluid phase consists of up to 10% CO_2 ($x_c \leq 0.1$). We therefore used initial conditions that are equivalent to $p_{H_2O} = 50$ MPa and $x_c = 0.1$ using the solubility model of *Liu et al.* [2005].

[49] The initial concentrations of dissolved H_2O and CO_2 are $c_{(w,0)} = 2.62$ wt.% and $c_{(c,0)} = 34$ ppm, respectively. The corresponding equilibrium solubility pressure is $p_{sol} = 55.52$ MPa. We used an initial bubble radius of $R_0 = (1 + \gamma)\, 2\sigma/p_{sol}$ (section 4) at an internal pressure $p_g = p_{sol}$, where $\gamma = 10^{-2}$. We assumed a constant value of $\sigma = 0.08$ N m^{-1} [*Gardner and Ketcham*, 2011, and references therein], because model results are not significantly sensitive to σ, within the range of measured values (Figures 5 and 6). Furthermore, we assumed a constant ambient pressure, $p_m = 10^5$ Pa, for the bubble growth calculations.

7.2. Modeling the Volume Fraction Density, $\phi(a_i)$

[50] Using these initial and boundary conditions, we modeled bubble growth for individual bubbles, j, each of which is surrounded by a given volume of melt, $v_{m,j}$. Each bubble undergoes a distinct growth history, beginning at time $t = t_f - \tau_j$ (Figure 8) and resulting in a final vesicle size, $R_j(\tau_j)$, after a growth time, τ_j. The values of τ_j and $R_j(\tau_j)$ were determined from the condition that

$$c_{(w,r=S)} = (1 - \epsilon)\, c_{(w,0)}, \tag{29}$$

where $\epsilon \ll 1$ assures that the condition of Equation (29) represents the threshold at which diffusion begins to affect the entire volume of melt, that is when J begins to decrease rapidly (Figures 8 and 9). Furthermore, the requirement that $c_{(w,r=S)}$ is the same for all bubbles assures that the concentration of H_2O between any two bubbles is continuously smooth. Because the diffusivity of CO_2 is considerably smaller than H_2O diffusivity, we found that $c_{(c,r=S)} = c_{(c,0)}$ for all of our calculations (Figure 10).

[51] Using smooth cubic spline interpolation of the discrete values $R_j = f(\tau_j)$, we obtained the functions $R = f_R(\tau)$ (Figure 11), and from the relation

$$v_{m,j} = \frac{4\pi}{3}\left[S_j(t)^3 - R_j(t)^3\right], \tag{30}$$

we similarly obtained $S = f_S(\tau)$.

[52] We then find the values of $\tau = \tau_i$, corresponding to the condition $f_R(\tau_i) = a_i$. Defining $R_i = f_R(\tau_i)$ and $S_i = f_S(\tau_i)$, we calculated the predicted volume fraction of vesicles (Figure 12) from

$$\phi_{mod} = \sum_i \phi_{mod}(a_i) = \sum_i \left[n(a_i) \left(\frac{R_i}{S_i}\right)^3 \right]. \tag{31}$$

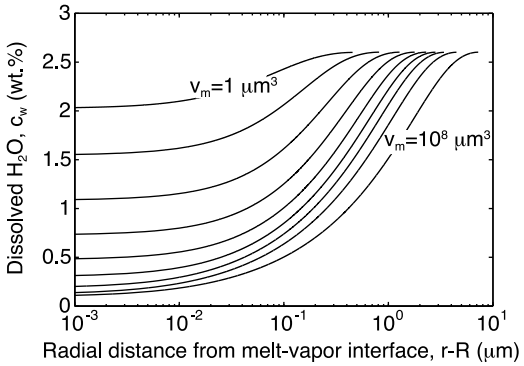

Figure 9. Concentration of dissolved H_2O in weight percent (wt.%) at time τ_j after nucleation, for bubbles with $v_{m,j} = 10^0$, 10^1.. 10^8 μm^3 as a function of radial distance from the melt-vapor interface, r-R, of the growing bubble.

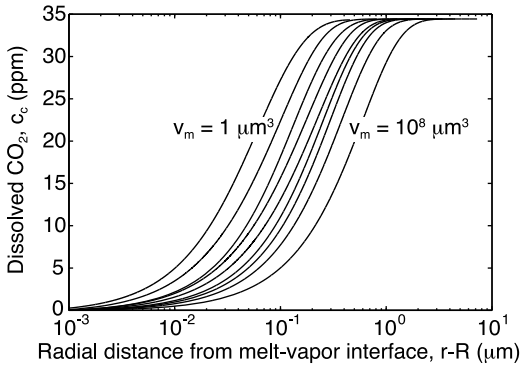

Figure 10. Concentration of dissolved CO_2 in parts per million (ppm) at time τ_j after nucleation, for bubbles with $v_{m,j} = 10^0, 10^1 .. 10^8$ μm^3 as a function of radial distance from the melt-vapor interface, *r-R*, of the growing bubble.

[53] We repeated the steps outlined in this section iteratively for different values of ϵ until the misfit between modeled and measured volume fraction, $|\phi_{mod} - \phi_{sam}|$ was minimized. We found that $10^{-3} \leq \epsilon \leq 10^{-2}$ provides a good fit (Figure 13). The resultant volume fraction density distributions, $\phi_{mod}(a_i)$, together with the actual distributions, $\phi_{sam}(a_i)$, are shown in Figure 12.

7.3. Nucleation Rate, $J(t)$, and Pressure, $p_m(t)$

[54] Using the functional relation $f_R(\tau)$ at values of $R = a_i$ and a smooth cubic spline interpolation, we obtain $N(t) = N(t_f - \tau)$ from the discrete distribution $N(a_i)$. We then calculate the time-dependent nucleation rate, $J(t)$, from $N(t)$ using Equation (19). The results are shown in Figure 14.

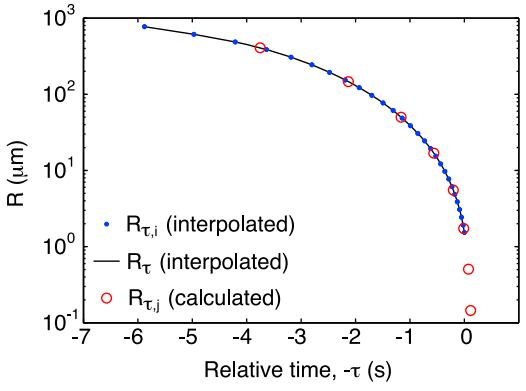

Figure 11. Modeled and interpolated values of R_j, R_i and R versus τ_j, τ_i and τ, respectively (sample 94-Z-22-24).

[55] Assuming that the maximum value of $J(t)$ occurs at $\Delta P_s = P_{ch}$, we calculate σ_e using Equation (6) and subsequently $\Delta P_s(t)$ from $J(t)$ using Equation (20). The results are shown in Figure 15.

8. Discussion

8.1. Nucleation and Decompression Rates

[56] Modeling of vesicle size distributions measured in Novarupta dacite clasts 94-Z-22-8, 94-Z-22-24 and 94-Z-22-28 (Figure 12) provides constraints on nucleation rate (Figure 14) and decompression rate (Figure 15). The three clasts span a range in vesicularity (ϕ = 0.52, 0.64 and 0.75) within a single tephro-stratigraphic level, interpreted in terms of radial variability within the conduit [*Adams et al.*, 2006]. We find that the observed textural variability requires approximately 25% variability (≈1 MPa s^{-1}) in decompression rate. The estimated peak nucleation rates are similar to the predictions by *Toramaru* [1989, 1995, 2006], but at decompression rates of $<10^7$ Pa s^{-1}, which are considerably lower than those predicted by *Toramaru* [1989,

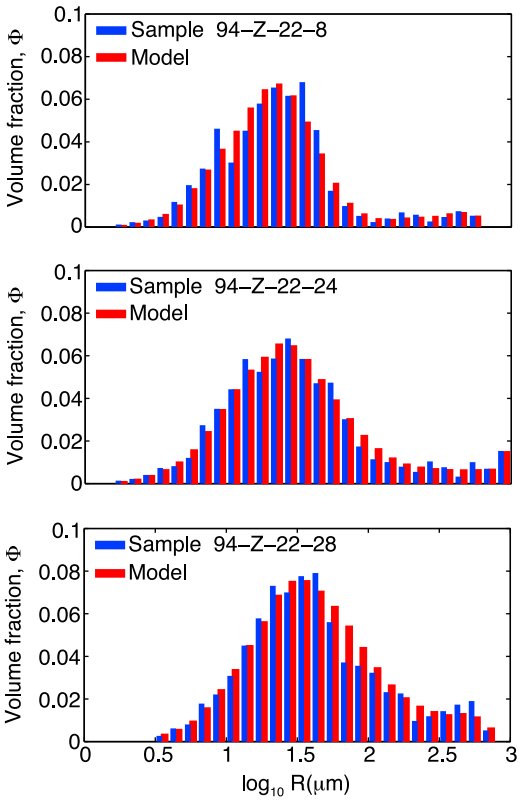

Figure 12. Comparison of modeled ($\phi_{mod}(a_i)$) and actual ($\phi_{sam}(a_i)$) distributions of vesicle volume fraction of Novarupta samples 94-Z-22-8, 24 and 28 (ϕ = 0.52, 0.64 and 0.75, respectively).

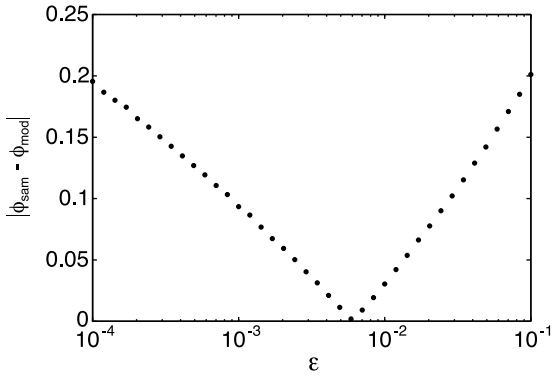

Figure 13. Misfit $|\phi_{mod} - \phi_{sample}|$ for sample 94-Z-22-24 as a function of the parameter ϵ (Equation (29)).

1995, 2006] and more consistent with conduit flow models [e.g., *Koyaguchi*, 2005; *Massol and Koyaguchi*, 2005].

[57] The model makes no assumptions about where or when bubble nucleation takes place, relative to fragmentation. We find that the peak in nucleation coincides with a peak in volumetrically averaged bubble overpressure and values that are approximately equal to empirical overpressures at which fragmentation is predicted (see section 8.2 for a detailed discussion). Unless fragmentation occurred by some other mechanism than postulated by current fragmentation models [e.g., *Spieler et al.*, 2004a; *Mueller et al.*, 2008], the most plausible explanation would be that the predicted coincident peaks in bubble overpressure and nucleation also coincided with fragmentation. In other words, bubble nucleation and fragmentation occur in very close temporal succession, suggesting that both feed back upon one another.

8.2. Magma Fragmentation

[58] The Novarupta dacite VSDs indicate magmatic conditions close to the critical stress threshold for magma fragmentation (Figure 16). The fragmentation stress threshold predicts brittle fracture of bubble walls, once $(p_g - p_m)$ exceeds a critical value [e.g., *Alidibirov*, 1994; *Zhang*, 1999; *Spieler et al.*, 2004a; *Mueller et al.*, 2008]. This threshold, expressed in terms of a potential energy, Ψ_{fr}, increases with sample porosity, ϕ, because the potential energy, Ψ, of the compressed volatiles within a given volume of magma increases with ϕ. In addition, the thickness of the melt that surrounds individual bubbles, whose tensile strength must be exceeded for fragmentation, decreases with increasing ϕ. However, as ϕ increases, more bubbles become interconnected, thereby increasing permeability, k. Because permeable outgassing dissipates overpressure, Ψ_{fr} also depends on k, and has been determined empirically by *Mueller et al.* [2008] as

$$\Psi_{fr} = 8.21 \times 10^{11}\sqrt{k} + 1.54 \times 10^{6} \quad \text{in units of J m}^{-3}. \quad (32)$$

[59] We find that the maximum volumetrically averaged bubble overpressure occurs when the model matches the vesicle size distributions preserved in the Novarupta pumice samples. If the associated potential energy was sufficient to cause magma fragmentation, magma permeability prior to fragmentation must have had values of $k \ll 10^{-13}$ m^2 (dashed lines in Figure 16, see also discussion in section 8.5). Nucleation of the vast majority of bubbles took place within ~0.1 s, perhaps not much longer than the time it takes for magma to traverse the fragmentation 'level' [*Spieler et al.*, 2004b]. Consistent with the work by *Massol and Koyaguchi*

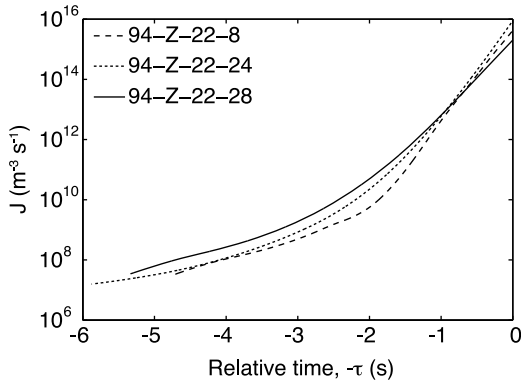

Figure 14. Predicted nucleation rates, J, as a function of $-\tau$.

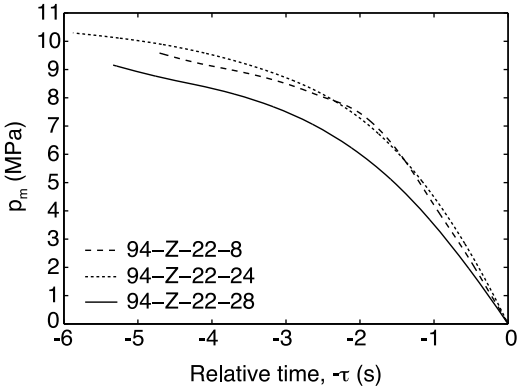

Figure 15. Predicted ambient pressure, p_m, as a function of $-\tau$.

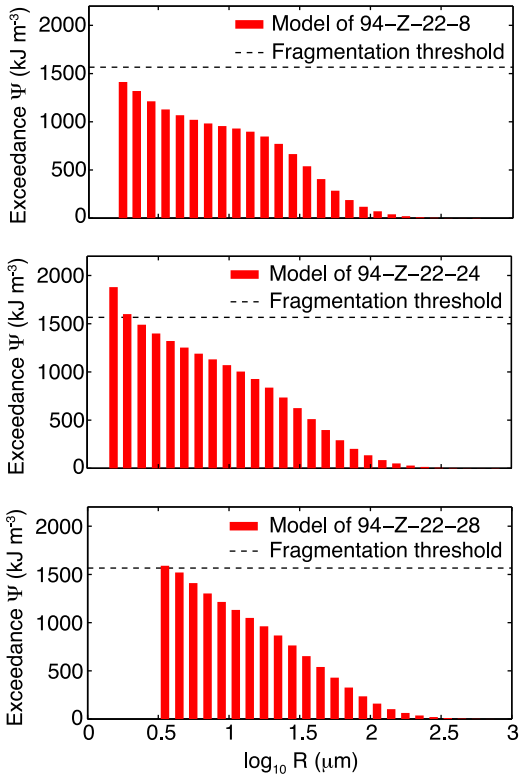

Figure 16. The potential energy for fragmentation, Ψ, is calculated using Equation 14 of *Alidibirov* [1994] and the fragmentation threshold is based on the empirical formulation of *Mueller et al.* [2008] at a permeability of $\ll 10^{-13}$ m^2.

[2005], this implies that nucleation proceeded until fragmentation, and supports the notion that feedbacks between bubble nucleation and fragmentation are self-sustaining processes, with the peak in nucleation rate more or less coinciding with fragmentation.

8.3. Magma Ascent Rates

[60] Magma ascent rates below the depth of fragmentation, u, can be calculated from the estimated decompression rates, dp_m/dt, where

$$\frac{dp_m}{dt} = \frac{dz}{dt}\frac{dp_m}{dz} = u\frac{dp_m}{dz} = u\left(\frac{dp_m}{dz}\right)_\rho + u\left(\frac{dp_m}{dz}\right)_\eta. \quad (33)$$

Here,

$$\left(\frac{dp_m}{dz}\right)_\rho = (1-\phi)\rho_m g \sim 10^4 \text{ Pa} \quad (34)$$

magma-static pressure loss and

$$\left(\frac{dp_m}{dz}\right)_\eta = 2(1-\phi)\,\rho_m u^2 \frac{f}{d} \quad (35)$$

is the viscous pressure loss. d is the conduit diameter and f is the friction factor

$$f = \frac{16}{Re} + f_0. \quad (36)$$

Re = $ud\rho_m(1-\phi)/\eta$ is the Reynolds number and f_0 has values of about 0.002–0.02 [e.g., *Mastin and Ghiorso*, 2000]. Thus

$$\frac{dp_m}{dt} = u(1-\phi)\,\rho_m g + 32u^2\frac{\eta}{d^2} + 2u^3(1-\phi)\,\rho_m\frac{f_0}{d}. \quad (37)$$

At the observed values of ϕ, predicted values of dp_m/dt (Figure 15), likely values of $d \sim 100$ m [*Hildreth and Fierstein*, 2012], as well as $\eta > 10^5$ Pa s (Figure 7) [*Hui and Zhang*, 2007], predicted magma ascent rates just below the fragmentation depth are $\sim$10 m s^{-1}.

8.4. Bubble Coalescence

[61] The minimum bubble wall thickness in silicic melts, before spontaneous rupture and coalescence, is thought to be $\sim$1 μm or less [e.g., *Klug and Cashman*, 1996; *Navon and Lyakhovsky*, 1998]. Given a magma viscosity of $\sim 10^5$ Pa s (Figure 7), the time required for capillary or gravitational thinning of bubble walls is too long to be of significance for the Novarupta dacites. Instead, coalescence is expected to be the consequence of bubble-wall thinning as a consequence of bubble growth (C. Nguyen et al. The lifetime of bubbles: film drainage and bubble coalescence, submitted to *Geochemistry, Geophysics, Geosystems*, 2012).

[62] Although we presently lack quantitative a-priori constraints on bubble coalescence rates during bubble growth, bubble shapes potentially provide a record thereof. After the melt film that separates adjacent bubbles ruptures and bubbles coalesce, capillary stress deforms bubbles back toward a spherical shape. This process is sometimes referred to as shape relaxation and occurs over a characteristic timescale [e.g., *Gardner*, 2007b]

$$\tau_{\text{relax}} \sim \frac{\eta R}{\sigma}. \quad (38)$$

[63] For Novarupta dacite with $R \geq 10^{-6}$ m, we find that $\tau_{\text{relax}} \geq 1$. It is therefore likely that textural evidence for coalescence should be preserved within pyroclasts [e.g., *Klug and Cashman*, 1996; *Gardner*, 2007b]. The VSDs modeled herein are based on a methodology whereby multiple coalesced vesicles with incomplete shape relaxation are treated as multiple individual vesicles [*Adams*

et al., 2006]. Therefore, not modeling coalescence represents a reasonable approximation, especially for the smallest (i.e., youngest) vesicles.

8.5. Open-System Degassing

[64] The predicted onset of magma fragmentation requires the exsolution of only 10–20% of the pre-eruptive magmatic volatiles (Figures 9 and 10). We have measured approximately 2.4 wt.% H_2O in the Novarupta dacite pumice samples, but it is unclear how much of this H_2O is of magmatic origin, as opposed to from rehydration by atmospheric H_2O (T. Giachetti and H. M. Gonnermann, Water in pumices: Rehydration versus incomplete degassing, submitted to *Earth and Planetary Science Letters*, 2012). Unless Novarupta pumice samples retain a large fraction of pre-eruptive magmatic volatiles within their matrix glass, degassing of most of these volatiles requires some degree of open-system gas loss, either before, during or after fragmentation. Open-system gas loss requires that coalescing bubbles form a continuous network of interconnected bubbles through which magmatic gas can flow. This is thought to occur at $\phi \geq 0.3$ [e.g., *Rust and Cashman*, 2004; *Wright et al.*, 2009; *Rust and Cashman*, 2011]. Our bubble growth calculations assume a closed system (section 6.3.3). This is valid if there is insufficient time for gas to escape prior to magma fragmentation and will be substantiated in the subsequent paragraphs.

[65] An estimate for the rate of permeable gas flux can be obtained from Forchheimer's equation [*Forchheimer*, 1901; *Innocentini et al.*, 1998; *Rust and Cashman*, 2004]

$$\frac{p_g}{L} \sim \frac{\eta_g}{k_1 \rho_g} q_g + \frac{1}{k_2 \rho_g} q_g^2, \tag{39}$$

where it is assumed that gas flow is caused by a pressure difference of the order of p_g over a characteristic length of L. Here, q_g is the mass flux of gas, $\eta \sim 10^{-5}$ Pa s is gas viscosity [e.g., *Takeuchi et al.*, 2009; *Rust and Cashman*, 2004, 2011], $\rho_g = p_g m_g / R_g T$ is gas density, $m_g \sim 10^{-2}$ kg mol^{-1} is the molar mass of the gas phase, $R_g = 8.314$ J mol^{-1} K^{-1} is the universal gas constant, and T is the temperature. In addition, k_1 is the viscous (Darcian) permeability and k_2 is the inertial (non-Darcian) permeability, which can be approximated as $k_2 = 4.75 \times 10^{14} (k_1)^{1.87}$ [*Rust and Cashman*, 2004].

[66] The advective mass flux of dissolved volatiles, carried upward with the ascending magma at velocity u, is given by

$$q_m \sim u \rho_m \left(c_{(w,0)} + c_{(c,0)} \right). \tag{40}$$

For estimated magma ascent rates of $u \sim 10$ m s^{-1} and $c_{(w,0)} + c_{(c,0)} \sim 10^4$ ppm, Equation (40) gives $q_m \sim 10^2$ kg s^{-1} m^{-2}.

[67] A conservative requirement for open-system gas loss not to be negligible is that

$$q_g \geq 0.1 q_m. \tag{41}$$

For a relatively high value of $k_1 \sim 10^{-12}$ m^2 [e.g., *Rust and Cashman*, 2004; *Wright et al.*, 2009; *Rust and Cashman*, 2011], $m_g \sim 10^{-2}$ kg mol^{-1}, the inequality of Equation (41) gives the minimum constraint that $q_g \geq 10$ kg s^{-1} m^{-2}, which indicates that the last term in Equation (39) is dominant [*Degruyter et al.*, 2012], that is

$$\frac{\eta_g}{k_1 \rho_g} q_g \ll \frac{1}{k_2 \rho_g} q_g^2. \tag{42}$$

Consequently, from Equation (41)

$$\sqrt{\frac{p_g k_2 \rho_g}{L}} \geq 10 \ \text{kg m}^{-2} \text{s}^{-1}, \tag{43}$$

or

$$\sqrt{L} \leq \frac{p_g}{10^8 \ \text{Pa m}^{-1/2}}. \tag{44}$$

[68] This inequality is difficult to satisfy below the fragmentation depth and the assumption of closed-system degassing to this point is therefore justified. Only within a very short distance of the 'fragmentation surface' will permeable gas loss become significant [*Mueller et al.*, 2008]. For example, at pressures near the fragmentation value, that is $p_g \sim 10^7$ Pa, permeable gas loss becomes important within $L \sim 10^{-2}$ m of the fragmentation surface or, equivalently, during the last $\sim 10^{-3}$ s prior to fragmentation. It should be noted that $k_1 \sim 10^{-12}$ m^2 is a conservatively high value and that values of $k_1 \sim 10^{-13}$ m^2 are probably more reasonable to assume at fragmentation.

[69] Once the magma has fragmented, $L \sim 10^{-2}$ m [e.g., *Rust and Cashman*, 2011; *Dufek et al.*, 2012], and Equation (39) indicates that open-system degassing of pyroclasts will be efficient over a wide range of values of p_g. Thus, unless the matrix glasses of the 1912 Novarupta dacite pyroclasts contain

a large fraction of the pre-eruptive volatiles, the majority of magmatic volatiles must have been lost after magma fragmentation and prior to quenching [e.g., *Thomas et al.*, 1994; *Gardner et al.*, 1996; *Kaminski and Jaupart*, 1997, 1998; *Tait et al.*, 1998; *Xu and Zhang*, 2002; *Burgisser and Gardner*, 2005; *Takeuchi et al.*, 2009], through combined volatile exsolution and open-system gas loss. If this is the case, and if open-system gas loss is sufficiently fast to balance exsolution, there may be negligible change in bubble size over viscous timescales of $\eta R/\sigma \gtrsim 10$ s.

9. Conclusions

[70] Vesicle size distributions in pumice provide a direct record of the dynamics of magma ascent. For a given parcel of magma, ascent-driven decompression produces increasing volatile supersaturation and bubble nucleation rates. Older bubbles grow larger, because volatiles diffuse into the bubble from a larger volume of melt. Those portions of the melt not yet affected by diffusion into existing bubbles remain fully saturated and comprise a region where bubbles continue to nucleate. Once volatile concentrations begin to decrease throughout the entire melt volume, bubble nucleation rates diminish rapidly.

[71] The fundamental approximation of our modeling approach is that the time when nucleation ceases is a common time for all bubbles within a given volume of melt, regardless of their time of nucleation. Pegging this time for any bubble, permits the reconstruction of a nucleation history. Our model accounts for the joint exsolution of H_2O and CO_2 and we find that main effect of CO_2 is to decrease the rates at which bubbles grow after nucleation. However, because of the relatively low CO_2 concentrations in Novarupta dacites, this effect is not of importance.

[72] Because we estimate bubble nucleation rates from precise diffusive bubble growth calculations, we minimize the large uncertainties associated with surface tension. We predict magma decompression rates of the order of 10^7 Pa s^{-1}, consistent with conduit flow models [e.g., *Koyaguchi*, 2005; *Massol and Koyaguchi*, 2005] and approximately one order of magnitude lower than would be predicted by the bubble number density decompression rate meter of *Toramaru* [2006]. Our modeled vesicle size distributions for the Novarupta dacite samples are consistent with conditions that correspond to the potential energy threshold for magma fragmentation. Therefore, the highest nucleation rates appear to coincide with magma fragmentation, supporting the notion that feedbacks between both processes are potentially self-sustaining [e.g., *Massol and Koyaguchi*, 2005].

[73] In 1912 Novarupta dacite that formed the pyroclasts analyzed herein, bubble growth was rapid. The smallest vesicles, which are also the most abundant, grew to their final size within a few hundred milliseconds. Interestingly, our model results suggest that only a fraction of the pre-eruptive dissolved volatiles, that is 10–20%, is exsolved from the melt at the time of magma fragmentation. The implication is that the 1912 Novarupta pyroclasts either retain a substantial amount of magmatic volatiles in their matrix glass, or that the majority of magmatic volatiles was lost by open-system degassing after magma fragmentation and before quenching.

Acknowledgments

[74] HMG was supported by NSF grant EAR-1019872. We thank H. M. N. Wright and J. M. Castro for thorough and helpful reviews. We acknowledge the major roles of W. Hildreth, J. Fierstein and C. J. N. Wilson in earlier studies of the dynamics of the 1912 Novarupta eruption and the painstaking work of N. K. Adams in processing the pyroclasts for vesicle size distribution.

References

Adams, N. K., B. F. Houghton, and W. Hildreth (2006), Abrupt transitions during sustained explosive eruptions: Examples from the 1912 eruption of Novarupta, Alaska, *Bull. Volcanol.*, *69*, 189–206.

Alidibirov, M. (1994), A model for viscous magma fragmentation during volcanic blasts, *Bull. Volcanol.*, *56*, 459–465.

Amon, M., and C. D. Denson (1984), A study of the dynamics of foam growth: analysis of the growth of closely spaced spherical bubbles, *Polymer Eng. Sci.*, *24*, 1026–1034.

Arefmanesh, A., and S. Advani (1991), Diffusion-induced growth of a gas bubble in a viscoelastic fluid, *Rheol. Acta*, *30*, 274–283.

Bagdassarov, N. S., A. Dorfman, and D. B. Dingwell (2000), Effect of alkalis, phosphorus, and water on the surface tension of haplogranite melt, *Am. Mineral.*, *85*, 33–40.

Bai, L., D. Baker, and M. Rivers (2008), Experimental study of bubble growth in Stromboli basalt melts at 1 atm, *Earth Planet. Sci. Lett.*, *267*, 533–547.

Blower, J. D., J. P. Keating, H. M. Mader, and J. C. Phillips (2001a), Inferring volcanic degassing processes from vesicle size distributions, *Geophys. Res. Lett.*, *28*, 347–350.

Blower, J. D., H. M. Mader, and S. D. R. Wilson (2001b), Coupling of viscous and diffusive controls on bubble growth during explosive volcanic eruptions, *Earth Planet Sci. Lett.*, *193*, 47–56.

Blower, J. D., J. P. Keating, H. M. Mader, and J. C. Phillips (2002), The evolution of bubble size distributions in volcanic eruptions, *J. Volcanol. Geotherm. Res.*, *120*, 1–23.

Blundy, J., K. V. Cashman, A. Rust, and F. Witham (2010), A case for CO2-rich arc magmas, *Earth Planet. Sci. Lett.*, *290*, 289–301.

Borkovec, M., W. de Paris, and R. Peikert (1994), The fractal dimension of the Apollonian sphere packing, *Fractals*, *2*, 521–526.

Burgisser, A., and J. E. Gardner (2005), Experimental constraints on degassing and permeability in volcanic conduit flow, *Bull. Volcanol.*, *67*, 42–56.

Burgisser, A., B. Scaillet, and Harshvardhan (2008), Chemical patterns of erupting silicic magmas and their influence on the amount of degassing during ascent, *J. Geophys. Res.*, *113*, B12204, doi:10.1029/2008JB005680.

Chouet, B., P. Dawson, and M. Nakano (2006), Dynamics of diffusive bubble growth and pressure recovery in a bubbly rhyolitic melt embedded in an elastic solid, *J. Geophys. Res.*, *111*, B07310, doi:10.1029/2005JB004174.

Cluzel, N., D. Laporte, A. Provost, and I. Kannewischer (2008), Kinetics of heterogeneous bubble nucleation in rhyolitic melts: Implications for the number density of bubbles in volcanic conduits and for pumice textures, *Contrib. Mineral. Petrol.*, *156*, 745–763.

Degruyter, W., O. Bachmann, A. Burgisser, and M. Manga (2012), The effects of outgassing on the transition between effusive and explosive silicic eruptions, *Earth Planet. Sci. Lett.*, *349–350*, 161–170.

Dingwell, D. B. (1996), Volcanic dilemma: Flow or blow?, *Science*, *273*, 1054–1055.

Dufek, J., M. Manga, and A. Patel (2012), Granular disruption during explosive volcanic eruptions, *Nat. Geosci.*, *5*, 561–564.

Epel'baum, M. B., I. V. Babashov, and T. P. Salova (1973), Surface tension of felsic magmatic melts at high temperatures and pressures, *Geochem. Int.*, *10*, 343–345.

Fierstein, J., and W. Hildreth (1992), The plinian eruptions of 1912 at Novarupta, Katmai National Park, Alaska, *Bull. Volcanol.*, *54*, 646.

Forchheimer, P. (1901), Wasserbewegung durch Boden, *Z. Ver. Dtsch. Ing.*, *45*, 1781–1788.

Gaonac'h, H., S. Lovejoy, J. Stix, and D. Schertzer (1996), A scaling growth model for bubbles in basaltic lava flows, *Earth Planet. Sci. Lett.*, *139*, 395–409.

Gaonac'h, H., S. Lovejoy, and D. Schertzer (2003), Percolating magmas and explosive volcanism, *Geophys. Res. Lett.*, *30*(11), 1559, doi:10.1029/2002GL016022.

Gaonac'h, H., S. Lovejoy, and D. Schertzer (2005), Scaling vesicle distributions and volcanic eruptions, *Bull. Volcanol.*, *67*, 350–357.

Gardner, J. E. (2007a), Heterogeneous bubble nucleation in highly viscous silicate melts during instantaneous decompression from high pressure, *Chem. Geol.*, *236*, 1–12.

Gardner, J. E. (2007b), Bubble coalescence in rhyolitic melts during decompression from high pressure, *J. Volcanol. Geotherm. Res.*, *166*, 161–176.

Gardner, J. E., and M. H. Denis (2004), Heterogeneous bubble nucleation on Fe-Ti oxide crystals in high-silica rhyolitic melts, *Geochim. Cosmochim. Acta*, *68*, 3587–3597.

Gardner, J. E., and R. A. Ketcham (2011), Bubble nucleation in rhyolite and dacite melts: Temperature dependence of surface tension, *Contrib. Mineral. Petrol*, *162*, 929–943.

Gardner, J. E., R. M. E. Thomas, and C. Jaupart (1996), Fragmentation of magma during Plinian volcanic eruptions, *Bull. Volcanol.*, *58*, 144–162.

Gardner, J. E., M. Hilton, and M. R. Carroll (1999), Experimental constraints on degassing of magma: Isothermal bubble growth during continuous decompression from high pressure, *Earth. Planet. Sci. Lett.*, *168*, 201–218.

Giachetti, T., T. H. Druitt, A. Burgisser, L. Arbaret, and C. Galven (2010), Bubble nucleation, growth and coalescence during the 1997 Vulcanian explosions of Soufrière Hills Volcano, Montserrat, *J. Volcanol. Geotherm. Res.*, *193*, 215–231.

Giachetti, T., A. Burgisser, L. Arbaret, T. H. Druitt, and K. Kelfoun (2011), Quantitative textural analysis of Vulcanian pyroclasts (Montserrat) using multi-scale X-ray computed microtomography: Comparison with results from 2D image analysis, *Bull. Volcanol.*, *73*, 1295–1309.

Gonde, C., C. Martel, M. Pichavant, and H. Bureau (2011), In situ bubble vesiculation in silicic magmas, *Am. Mineral.*, *96*, 111–124.

Gonnermann, H. M., and M. Manga (2005), Nonequilibrium magma degassing: Results from modeling of the ca.1340 AD eruption of Mono Craters, California, *Earth. Planet. Sci. Lett.*, *238*, 1–16.

Gonnermann, H. M., and M. Manga (2007), The fluid mechanics inside a volcano, *Annu. Rev. Fluid Mech.*, *39*, 321–356.

Gurioli, L., B. F. Houghton, K. V. Cashman, and R. Cioni (2005), Complex changes in eruption dynamics during the 79 AD eruption of Vesuvius, *Bull. Volcanol.*, *67*, 144–159.

Hamada, M., D. Laporte, N. Cluzel, K. T. Koga, and T. Kawamoto (2010), Simulating bubble number density of rhyolitic pumices from Plinian eruptions: Constraints from fast decompression experiments, *Bull. Volcanol.*, *72*, 735–746

Hammer, J. E., K. V. Cashman, R. P. Hoblitt, and S. Newman (1999), Degassing and microlite crystallization in pre-climactic events of the 1991 eruption of Mt. Pinatubo, Philippines, *Bull. Volcanol.*, *60*, 355–380.

Hammer, J. E., M. J. Rutherford, and W. Hildreth (2002), Magma storage prior to the 1912 eruption at Novarupta, Alaska, *Contrib. Mineral. Petrol.*, *144*, 144–162.

Herd, R. A., and H. Pinkerton (1997), Bubble coalescence in basaltic lava: Its impact on the evolution of bubble populations, *J. Volcanol. Geotherm. Res.*, *75*, 137–157.

Hildreth, W. (1983), The compositionally zoned eruption of 1912 in the valley of ten thousand smokes, Katmai National Park, Alaska, *J. Volcanol. Geotherm. Res.*, *18*, 1–56.

Hildreth, W., and J. Fierstein (2000), Katmai volcanic cluster and the great eruption of 1912, *Geol. Soc. Am. Bull.*, *112*, 1594–1620.

Hildreth, W., and J. Fierstein (2012), The Novarupta-Katmai eruption of 1912– Largest eruption of the twentieth century: Centennial perspectives, *U.S. Geol. Surv. Prof. Pap.*, *1791*, 259.

Hirth, J. P., G. M. Pound, and G. R. St Pierre (1970), Bubble nucleation, *Metall. Trans.*, *1*, 939–945.

Houghton, B. F., R. J. Carey, K. V. Cashman, C. J. N. Wilson, B. J. Hobden, and J. E. Hammer (2010), Diverse patterns of ascent, degassing, and eruption of rhyolite magma during the 1.8 ka Taupo eruption, New Zealand: Evidence from clast vesicularity, *J. Volcanol. Geotherm. Res.*, *195*, 31–47.

Hui, H. J., and Y. X. Zhang (2007), Toward a general viscosity equation for natural anhydrous and hydrous silicate melts, *Geochim. Cosmochim. Acta*, *71*, 403–416.

Hurwitz, S., and O. Navon (1994), Bubble nucleation in rhyolitic melts–Experiments at high-pressure, temperature, and water-content, *Earth. Planet. Sci. Lett.*, *122*, 267–280.

Innocentini, M. D. M., P. Sepulveda, V. R. Salvini, V. C. Pandolfelli, and J. R. Coury (1998), Permeability and structure

of cellular ceramics: A comparison between two preparation techniques, *J. Am. Ceram. Soc.*, *81*, 3349–3352.
Kaminski, E., and C. Jaupart (1997), Expansion and quenching of vesicular magma fragments in Plinian eruptions, *J. Geophys. Res.*, *102*, 12,187–12,203.
Kaminski, E., and C. Jaupart (1998), The size distribution of pyroclasts and the fragmentation sequence in explosive volcanic eruptions, *J. Geophys. Res.*, *103*, 29,759–29,779.
Kedrinskiy, V. (2009), Hydrodynamic aspects of explosive eruptions of volcanoes: Simulation problems, *Shock Waves*, *18*, 451–464.
Kerrick, D. M., and G. K. Jacobs (1981), A modified Redlich-Kwong Equation for H_2O, CO_2, and H_2O-CO_2 mixtures at elevated pressures and temperatures, *Am. J. Sci.*, *281*, 735–767.
Klug, C., and K. V. Cashman (1994), Vesiculation of May 18, 1980, Mount St. Helens Magma, *Geology*, *22*, 468–472.
Klug, C., and K. V. Cashman (1996), Permeability development in vesiculating magmas: Implications for fragmentation, *Bull. Volcanol.*, *58*, 87–100.
Klug, C., K. V. Cashman, and C. R. Bacon (2002), Structure and physical characteristics of pumice from the climactic eruption of Mount Mazama (Crater Lake), Oregon, *Bull. Volcanol.*, *64*, 486–501.
Koyaguchi, T. (2005), An analytical study for 1-dimensional steady flow in volcanic conduits, *J. Volcanol. Geotherm. Res*, *143*, 29–52.
Larsen, J. F. (2008), Heterogeneous bubble nucleation and disequilibrium H_2O exsolution in Vesuvius K-phonolite melts, *J. Volcanol. Geotherm. Res.*, *175*, 278–288.
Larsen, J. F., and J. E. Gardner (2000), Experimental constraints on bubble interactions in rhyolite melts: Implications for vesicle size distributions, *Earth. Planet. Sci. Lett.*, *180*, 201–214.
Lautze, N. C., and B. F. Houghton (2007), Linking variable explosion style and magma textures during 2002 at Stromboli volcano, Italy, *Bull. Volcanol.*, *69*, 445–460.
Lensky, N., V. Lyakhovsky, and O. Navon (2001), Radial variations of melt viscosity around growing bubbles and gas overpressure in vesiculating magmas, *Earth Planet. Sci. Lett.*, *186*, 1–6.
Lensky, N. G., O. Navon, and V. Lyakhovsky (2004), Bubble growth during decompression of magma: experimental and theoretical investigation, *J. Volcanol. Geotherm. Res.*, *129*, 7–22.
Liu, Y., Y. X. Zhang, and H. Behrens (2005), Solubility of H_2O in rhyolitic melts at low pressures and a new empirical model for mixed H_2O-CO_2 solubility in rhyolitic melts, *J. Volcanol. Geotherm. Res.*, *143*, 219–235.
Lovejoy, S., H. Gaonac'h, and D. Schertzer (2004), Bubble distributions and dynamics: The expansion-coalescence equation, *J. Geophys. Res.*, *109*, B11203, doi:10.1029/2003JB002823.
Lowenstern, J. B. (1993), Evidence for a copper-bearing fluid in magma erupted at the Valley of Ten Thousand Smokes, Alaska, *Contrib. Mineral. Petrol.*, *114*, 409–421.
Lubetkin, S. D. (2003), Why is it much easier to nucleate gas bubbles than theory predicts?, *Langmuir*, *19*, 2575–2587.
Lyakhovsky, V., S. Hurwitz, and O. Navon (1996), Bubble growth in rhyolitic melts: Experimental and numerical investigation, *Bull. Volcanol.*, *58*, 19–32.
Mangan, M., and T. Sisson (2000), Delayed, disequilibrium degassing in rhyolite magma: Decompression experiments and implications for explosive volcanism, *Earth. Planet. Sci. Lett.*, *183*, 441–455.
Mangan, M. T., and K. V. Cashman (1996), The structure of basaltic scoria and reticulite and inferences for vesiculation, foam formation, and fragmentation in lava fountains, *J. Volcanol. Geotherm. Res.*, *73*, 1–18.
Mangan, M., and T. Sisson (2005), Evolution of melt-vapor surface tension in silicic volcanic systems: Experiments with hydrous melts, *J. Geophys. Res.*, *110*, B01202, doi:10.1029/2004JB003215.
Mangan, M. T., K. V. Cashman, and S. Newman (1993), Vesiculation of basaltic magma during eruption, *Geology*, *21*, 157–160.
Mangan, M. T., T. W. Sisson, and W. B. Hankins (2004), Decompression experiments identify kinetic controls on explosive silicic eruptions, *Geophys. Res. Lett.*, *31*, L08605, doi:10.1029/2004GL019509.
Massol, H., and T. Koyaguchi (2005), The effect of magma flow on nucleation of gas bubbles in a volcanic conduit, *J. Volcanol. Geotherm. Res.*, *143*, 69–88.
Mastin, L. G. (2002), Insights into volcanic conduit flow from an open-source numerical model, *Geochem. Geophys. Geosyst.*, *3*(7), 1037, doi:10.1029/2001GC000192.
Mastin, L. G., and M. S. Ghiorso (2000), A numerical program for steady-state flow of magma-gas mixtures through vertical eruptive conduits, *U.S. Geol. Surv. Open File Rep.*, *00-209*, 53.
McBirney, A. R., and T. Murase (1970), Factors governing the formation of pyroclastic rocks, *Bull. Volcanol.*, *34*, 372–384.
Melnik, O., A. A. Barmin, and R. S. J. Sparks (2005), Dynamics of magma flow inside volcanic conduits with bubble overpressure buildup and gas loss through permeable magma, *J. Volcanol. Geotherm. Res.*, *143*, 53–68.
Mourtada-Bonnefoi, C. C., and D. Laporte (1999), Experimental study of homogeneous bubble nucleation in rhyolitic magmas, *Geophys. Res. Lett.*, *26*, 3505–3508.
Mourtada-Bonnefoi, C. C., and D. Laporte (2002), Homogeneous bubble nucleation in rhyolitic magmas: An experimental study of the effect of H_2O and CO_2, *J. Geophys. Res.*, *107*(B4), 2066, doi:10.1029/2001JB000290.
Mourtada-Bonnefoi, C. C., and D. Laporte (2004), Kinetics of bubble nucleation in a rhyolitic melt: An experimental study of the effect of ascent rate, *Earth. Planet. Sci. Lett.*, *218*, 521–537.
Mueller, S., B. Scheu, O. Spieler, and D. B. Dingwell (2008), Permeability control on magma fragmentation, *Geology*, *36*, 399–402.
Navon, O., and V. Lyakhovsky (1998), Vesiculation processes in silicic magmas, in *The Physics of Explosive Volcanic Eruptions*, edited by J. S. Gilbert and D. W. Sparks, *Spec. Pub. Geol. Soc.*, *145*, 27–50.
Nowak, M., S. B. Cichy, R. E. Botcharnikov, N. Walker, and W. Hurkuck (2011), A new type of high-pressure low-flow metering valve for continuous decompression: First experimental results on degassing of rhyodacitic melts, *Am. Mineral.*, *96*, 1373–1380.
Papale, P. (1999), Numerical simulations of magma ascent along volcanic conduits, *Phys. Chem. Earth, Part A*, *24*, 957–961.
Papale, P., and M. Polacci (1999), Role of carbon dioxide in the dynamics of magma ascent in explosive eruptions, *Bull. Volcanol.*, *60*, 583–594.
Piochi, M., M. Polacci, G. De Astis, A. Zanetti, A. Mangiacapra, R. Vannucci, and D. Giordano (2008), Texture and composition of pumices and scoriae from the Campi Flegrei caldera (Italy): Implications on the dynamics of explosive eruptions, *Geochem. Geophys. Geosyst.*, *9*, Q03013, doi:10.1029/2007GC001746.

Polacci, M. (2005), Constraining the dynamics of volcanic eruptions by characterization of pumice textures, *Ann. Geophys.*, *48*, 731–738.

Polacci, M., P. Papale, and M. Rosi (2001), Textural heterogeneities in pumices from the climactic eruption of Mount Pinatubo, 15 June 1991, and implications for magma ascent dynamics, *Bull. Volcanol.*, *63*, 83–97.

Polacci, M., L. Pioli, and M. Rosi (2003), The Plinian phase of the Campanian Ignimbrite eruption (Phlegraean Fields, Italy): Evidence from density measurements and textural characterization of pumice, *Bull. Volcanol.*, *65*, 418–432.

Polacci, M., R. A. Corsaro, and D. Andronico (2006a), Coupled textural and compositional characterization of basaltic scoria: Insights into the transition from Strombolian to fire fountain activity at Mount Etna, Italy, *Geology*, *34*, 201–204.

Polacci, M., D. R. Baker, L. Mancini, G. Tromba, and F. Zanini (2006b), Three-dimensional investigation of volcanic textures by X-ray microtomography and implications for conduit processes, *Geophys. Res. Lett.*, *33*, L13312, doi:10.1029/2006GL026241.

Polacci, M., D. R. Baker, L. Mancini, S. Favretto, and R. J. Hill (2009), Vesiculation in magmas from Stromboli and implications for normal Strombolian activity and paroxysmal explosions in basaltic systems, *J. Geophys. Res.*, *114*, B01206, doi:10.1029/2008JB005672.

Proussevitch, A., D. Sahagian, and A. Anderson (1993), Dynamics of diffusive bubble growth in magmas: Isothermal case, *J. Geophys. Res.*, *98*, 22,283–22,307.

Proussevitch, A. A., D. L. Sahagian, and E. P. Tsentalovich (2007), Statistical analysis of bubble and crystal size distributions: Formulations and procedures, *J. Volcanol. Geotherm. Res.*, *164*, 95–111.

Ramkrishna, D. (2000), *Population Balances Theory and Applicantion to Particulate Systems in Engineering*, 355 pp., Academic, San Diego, Calif.

Randolph, A. D., and M. A. Larson (1971), *Theory of Particulate Processes*, 251 pp., Academic, New York.

Rust, A. C., and K. V. Cashman (2004), Permeability of vesicular silicic magma: Inertial and hysteresis effects, *Earth. Planet. Sci. Lett.*, *228*, 93–107.

Rust, A. C., and K. V. Cashman (2011), Permeability controls on expansion and size distributions of pyroclasts, *J. Geophys. Res.*, *116*, B11202, doi:10.1029/2011JB008494.

Sahagian, D. L., and A. A. Proussevitch (1998), 3D particle size distributions from 2D observations: Stereology for natural applications, *J. Volcanol. Geotherm. Res.*, *84*, 173–196.

Shea, T., B. F. Houghton, L. Gurioli, K. V. Cashman, J. E. Hammer, and B. J. Hobden (2010), Textural studies of vesicles in volcanic rocks: An integrated methodology, *J. Volcanol. Geotherm. Res.*, *190*, 271–289.

Simakin, A. G., P. Armienti, and M. B. Epel'baum (1999), Coupled degassing and crystallization: Experimental study at continuous pressure drop, with application to volcanic bombs, *Bull. Volcanol.*, *61*, 275–287.

Sparks, R. S. J. (1978), The dynamics of bubble formation and growth in magmas: A review and analysis, *J. Volconal. Geotherm. Res.*, *3*, 1–37.

Sparks, R., and S. Brazier (1982), New evidence for degassing processes during explosive eruptions, *Nature*, *295*, 218–220.

Spera, F. J. (2000), Physical properties of magma, in *Encyclopedia of Volcanoes*, edited by H. Sigurdsson, pp. 171–190, Academic, San Diego, Calif.

Spieler, O., B. Kennedy, U. Kueppers, D. B. Dingwell, B. Scheu, and J. Taddeucci (2004a), The fragmentation threshold of pyroclastic rocks, *Earth. Planet. Sci. Lett.*, *226*, 139–148.

Spieler, O., D. B. Dingwell, and M. Alidibirov (2004b), Magma fragmentation speed: an experimental determination, *J. Volcanol. Geotherm. Res.*, *129*, 109–123.

Tait, S., R. Thomas, J. Gardner, and C. Jaupart (1998), Constraints on cooling rates and permeabilities of pumice in an explosive eruption jet from colour and magnetic mineralogy, *J. Volcanol. Geotherm. Res.*, *86*, 79–91.

Takeuchi, S., A. Tomiya, and H. Shinohara (2009), Degassing conditions for permeable silicic magmas: Implications from decompression experiments withc onstant rates, *Earth Planet. Sci. Lett.*, *283*, 101–110.

Thomas, N., C. Jaupart, and S. Vergniolle (1994), On the vesicularity of pumice, *J. Geophys. Res.*, *99*, 15,633–15,644.

Toramaru, A. (1989), Vesiculation process and bubble-size distributions in ascending magmas with constant velocities, *J. Geophys. Res.*, *94*, 17,523–17,542.

Toramaru, A. (1990), Measurement of bubble size distributions in vesiculated rocks with implications for quantitative estimate ion of eruption processes, *J. Volcanol. Geotherm. Res.*, *43*, 71–90.

Toramaru, A. (1995), Numerical study of nucleation and growth of bubbles in viscous magmas, *J. Geophys. Res.*, *100*, 1913–1931.

Toramaru, A. (2006), BND (bubble number density) decompression rate meter for explosive volcanic eruptions, *J. Volcanol. Geotherm. Res.*, *154*, 303–316.

Voltolini, M., D. Zandomeneghi, L. Mancini, and M. Polacci (2011), Texture analysis of volcanic rock samples: Quantitative study of crystals and vesicles shape preferred orientation from X-ray microtomography data, *J. Volcanol. Geotherm. Res.*, *202*, 83–95.

Wallace, P. J. (2005), Volatiles in subduction zone magmas: concentrations and fluxes based on melt inclusion and volcanic gas data, *J. Volcanol. Geotherm. Res.*, *140*, 217–240.

Woods, A. W. (1995), The dynamics of explosive volcanic-eruptions, *Rev. Geophys.*, *33*, 495–530.

Wright, H. M. N., K. V. Cashman, E. H. Gottesfeld, and J. J. Roberts (2009), Pore structure of volcanic clasts: Measurements of permeability and electrical conductivity, *Earth Planet. Sci. Lett.*, *280*, 93–104.

Xu, Z., and Y. Zhang (2002), Quench rates in air, water, and liquid nitrogen, and inference of temperature in volcanic eruption columns, *Earth Planet. Sci. Lett.*, *200*, 315–330.

Yamada, K., H. Tanaka, K. Nakazawa, and H. Emori (2005), A new theory of bubble formation in magma, *J. Geophys. Res.*, *110*, B02203, doi:10.1029/2004JB003113.

Yamada, K., H. Emori, and K. Nakazawa (2008), Time-evolution of bubble formation in a viscous liquid, *Earth Planets Space*, *60*, 1–19.

Zhang, Y. X. (1999), A criterion for the fragmentation of bubbly magma based on brittle failure theory, *Nature*, *402*, 648–650.

Zhang, Y. X., and H. Ni (2010), Diffusion of H, C, and O components in silicate melts, *Rev. Mineral. Petrol.*, *72*, 171–225.

Zhang, Y. X., Z. J. Xu, M. F. Zhu, and H. Y. Wang (2007), Silicate melt properties and volcanic eruptions, *Rev. Geophys.*, *45*, RG4004, doi:10.1029/2006RG000216.